IEEE Access
Multidisciplinary ⋮ Rapid Review ⋮ Open Access Journal

Received 21 June 2024, accepted 18 July 2024, date of publication 29 July 2024, date of current version 13 August 2024.

Digital Object Identifier 10.1109/ACCESS.2024.3435569

RESEARCH ARTICLE

Balancing of Attenuation Disparity to Restore the Weak Color Channels in Underwater Images

M. KANAGAVEL AND V. THANIKAISELVAN, (Member, IEEE)
School of Electronics Engineering, Vellore Institute of Technology, Vellore, Tamil Nadu 632014, India
Corresponding author: V. Thanikaiselvan (thanikaiselvan@vit.ac.in)

ABSTRACT The images captured under water are typically deteriorated due to non uniform attenuation of traversing light in underwater medium. The studies on underwater environment mainly depends on the techniques for the enhancement of underwater images. Many state-of-the-arts compensate the losses due to scattering of light in underwater images but still it is a challenging task to compensate the color distortion due to absorption of light. A new approach is introduced in this article for the enhancement of underwater images by balancing the attenuation disparity between the color channels. This approach reduces the color dominancy based on the prior that the non-uniform attenuation of RGB channels of light in water which results in severely absorbed, moderately absorbed and informative color channels. The difference between the maximum pixel intensity level of an image and its color channels is considered as the attenuation disparity of color channels. So, this leads to the statistical classification of underwater images into five major types: haze, bluish, greenish, greenish blue and bluish green images and two special types such as yellowish image and dark image subjectively. The pixel intensity of severely and moderately absorbed color channels are manipulated in accordance with the informative color channel by adding the value of concerned attenuation disparity globally. It increases the pixel intensity level of weak color channels and restores the channel information but does not improve the visual quality. The Gray World (GW) method or color equalization (CE) method is applied to remove the color imbalance and the contrast is improved by saturating the high level and low level pixel intensities. Finally, the conventional multiscale image fusion is employed to improve the image quality. The experimental results show that the proposed method outperforms qualitatively and quantitatively in terms of underwater color image quality evaluation (UCIQE) metrics and underwater image quality measures (UIQM) compared to the existing image enhancement methods.

INDEX TERMS Attenuation disparity, attenuation of light, color equalization, Gray World assumption, image enhancement, underwater image classification.

I. INTRODUCTION

The scene information of an underwater image plays a major role in ocean related studies. The development of technology advances the autonomous underwater vehicles to capture images and videos without human intervention. However, the poor visibility of scenes in the captured underwater images is the main problem. The water medium absorbs the light energy, increases scattering and introduces noise which have direct negative impact on the quality of underwater images. Therefore, the images captured in underwater medium are deteriorated due to the attenuation of information carrying light by scattering and absorption i.e., nonuniform illumination. This results in color casts, low contrast, poor edges and corners and reduced visibility of underwater scene and other consequences are bright artefacts, over darkness, poor visibility of distant and background objects, blurriness and color distortions. These drawbacks limit the applications of computer vision in marine archaeology, ecology and rescue operations. The physics of attenuation of light in the water medium was studied experimentally by Ramaseshan [1], Duntley [2], Chilton et al. [3], and Wells [4]. Specifically, the

The associate editor coordinating the review of this manuscript and approving it for publication was Marco Giannelli.

scattering leads to poor visibility whereas absorption causes color distortion and loss of information as per the depth of the water medium [5]. In accordance with optical theory, the light with longer wavelength has less energy. Hence the wavelength of the visible spectrum is a factor for the disappearance of colors of light in the underwater medium. Therefore, the red spectrum disappears first since it has the longest wavelength (650-750 nm) and then the green color (550-650 nm) and finally the blue (450-550 nm). But this order of disappearance may vary depending upon the concentration of pollutants present in the underwater medium [3]. In the first case, the image appears in bluish green color or cyan color depending on the presence of concentration of pollutants. In the second case, almost the red disappears completely and the green color starts to disappear and hence the image looks blue or greenish blue color. In the third case, the blue color starts to disappear whereas the red and the green colors almost disappeared and hence the image appears in saturated blue color with black background regions. Sometimes, the underwater images captured near the coastal regions may appear in green color even in low depth due to the presence of heavy pollutants which make enfeeblement and early absorption of the blue spectrum. If the camera is placed just above the water surface in the air medium and focused on the shallow depth scenes in clear water during clear sky, then the image looks hazy since the water acts like haze between the target object and the camera. As per the above discussion, we can infer that the absorption of light in the underwater medium is non-uniform with irregular pattern of attenuation. Therefore, only the light which is not fully absorbed gets scattered in the underwater medium.

This article mainly focuses on the solution to the problem of color casts occurred in underwater images due to absorption of light in addition to the compensation of losses due to scattering of light. Most of the existing methods focused to compensate either the scattering loss or absorption loss occurred in underwater images. Although some methods focused on compensating both the losses, the enhanced images are affected by unwanted color shades or red color artefacts. Further, our previous work [91] restores the weak color channel in underwater images based only on two types of images and hence the existing methods are not applicable for all the degraded underwater images. This is because, the color of appearance of underwater images varies in accordance with the loss of color channel information. This article introduces a novel color correction method based on a new statistical approach for classification of underwater images. Since the proposed method compensates the color casts with reduced color artefacts, it is considered as the best method for the enhancement of underwater images. However, it does not perform well to enhance the images captured in dark underwater scenes with less artificial lighting.

This article has been framed as: literature review in Section II, statistical analysis of underwater images in Section III, classification of underwater Images in Section IV, Proposed color correction in Section V, Results and Discussion in Section VI and finally the paper is concluded in Section VII.

II. LITERATURE REVIEW

The previous studies on the underwater image enhancement are reviewed under three categories: a) Model Based Image Restoration, b) Image enhancement by pixel manipulation and c) Deep Learning (DL) based image enhancement.

A. PHYSICAL MODEL BASED IMAGE RESTORATION

Many researchers worked on the physical model of haze image formation [6], [7], [8] in air medium. The haze image (I) with pixel location (x, y) in air medium is mathematically represented with two components: the intensity of light reflected by the target object and received by the camera (J) and the scattered ambient light (L) in the line of sight:

$$I = J.t + L(1 - t) \tag{1}$$

where t is the transmission stated by the Lambert-Beer law which is a decaying exponential of the product of attenuation coefficient (ρ) and the distance $d\ (x)$ between the target scene and the image plane (scene depth):

$$t = exp(-\rho d\ (x)) \tag{2}$$

The restoration of degraded haze images has been proposed by accounting of surface shading [9] with refinement of (1), Dark Channel Prior (DCP) [10] and enhancement of (1) with absorption coefficient [11]. The white balancing technique was used instead of physical model for dehazing purposes [12]. The physical model for terrestrial images has been extended to the underwater images with some modifications such as Dehazing with refined transmission followed by color correction [13], refined depth map from pixel blurriness [14], selective channel compensation [15], refinement of transmission [16], combination of DCP and soft matting [17], predominant channel transmission estimation [18] and adaptive dehazing [19] to estimate the transmission for image restoration. The color compensation followed by multi scale retinex restoration was proposed in [20]. The variants of DCP have also been proposed for restoration of underwater images by researchers including red channel prior [21] to estimate the image depth particularly for the enhancement of artificially illuminated regions, image statistics based hierarchical estimation of veiling light [22] to avoid bright objects in the scene, adaptive fusion of two different transmission maps derived from optical model based method and pixel based method [23].

In context to the underwater medium, McGlamery [24] and Jaffe [25] formulated the computer modelling of underwater imaging systems. They have shown, the total radiance received by the camera is a linear combination of the direct part (I_{DC}), forward scattering part (I_{FC}) and backward scattering part (I_{BC}). Further, the linear combination is represented as

$$I = J.t + J.t * H + L - L.t \tag{3}$$

The first term on right hand side of (3) is I_{DC}, the second term is I_{FC} and the third term is I_{BC}. But these methods are complex to underwater images since the details such as the irradiance received by the image plane, the background ambient light and the transmissivity of the medium are to be estimated. The equation (3) was simplified by ignoring I_{BC} [26] to design a restoring filter for enhancing shallow water images. Underwater-DCP [27] is the concept of applying DCP only to green and blue channels instead of red to restore the scene radiance. The fusion of two derived inputs from a restored underwater image have been proposed [28] for effective improvement of the visual quality. The color channels have been improved using Affine transformation and pixel saturation with improved DCP by ignoring I_{FC} [86] using (3) for UIE. The method of color transfer followed by DCP was proposed to remove the artefacts [29] wherein the color channel characteristics of reference images are transferred to the test images to manipulate the image statistics to improve the quality of images captured in challengeable conditions such as night time, sandstorm, underwater, etc. The concept introduced in [29] was implemented for underwater images [30] along with the DCP however the over darkness appeared in the results.

B. IMAGE ENHANCEMENT BY PIXEL MANIPULATION

The physical model-free method of enhancement has been introduced based on mixing of colors by Kumar and Bhandari [31], Ancuti et al. [32], [33] and Tao et al. [34]. Enhanced image was obtained from twelve derived images [31] by adding of a portion of dominant color channel to the attenuated color channels. The information of green channel was fractionally added to weak red channel to restore the information [32] but it results in yellow shades of appearance. The white balancing of [32] was extended in [33] with gaussian filtered version of the same weak color channel to avoid yellow appearance. However, these methods were used as a preprocessing step for enhancement of weakly illuminated images as a color channel compensation (3C) to improve color constancy methods. Because of prime attenuations of the red color component in underwater images, the extraction of pixels having the same reflectance (Gray information) and discriminating the image noise becomes intricate. So, the color correction methods [37] based on gray information such as average scene reflectance is gray [35], average of differences of scene reflectance is shades of gray [36], average edge difference is achromatic [38] and eliminating nonuniform illumination by taking average of two adjacent points (edges) [39] are inadequate for effective color compensation. Although some researchers attempted the color correction [30] and [31], the color distortion was not completely reduced. The technique of capturing multiple images in different exposure interval is called exposure bracketing imaging and this technique has also been utilized for color correction [40]. The color has been compensated using pixel-wise estimated attenuation matrices [60]. The fusion of color transferred image, maximum attenuation map and local color balanced image have been performed for color compensation [61]. A multi stage enhancement method including color compensation, color correction, detail sharpening and contrast enhancement was proposed to improve the image quality [62]. The optimized transmission map-based image restoration followed by color correction [63] was proposed with the help of new DCP and modified white balancing techniques. A multi-step image enhancement technique [64] was proposed in which dehazing, color correction, image sharpening, multiscale fusion of gamma corrected image and contrast limited adaptive histogram equalized image (CLAHE [57]).

C. DEEP LEARNING (DL) BASED IMAGE ENHANCEMENT

The DL based enhancement has been proposed by many researchers such as CycleGAN with Underwater ResNet (UResNet) [41], CNN with Dense-Residual [43], UWGAN [44], feature concatenation of nine dense residual network [45], joint network for adaptive dehazing by luminance reconstruction network and color correction by chrominance network [46], four level fusion of heterogeneous features [47], DenseNet [48] and restoration of horizontal distortion [49]. The advantages of GANs in terms of visual quality and physical model based enhancement methods were inherited by a network called PUGAN [68]. The conjunction of dense channel attention module and position attention module was introduced in Underwater Attention-GAN [69] respectively for suppressing low profile feature map and avoiding over enhancement. The multi exposure images were synthesized from single image by a network called DPIENet [70] and used for image restoration. The optical properties of [24] and [25] were incorporated with the neural network HybrUR [71] for restoration of underwater images. A network called TOPAL [72] was proposed to improve the contrast by a multiscale deep module and to correct the color deviations by an aesthetic render module. Multiscale Dense GAN [44] with stabilized discriminator using spectral normalization was proposed for recovering the image details. A new comparative framework with supervised learning mode named CLUIE-Net [73] and a large underwater image dataset RQSD-UI was proposed for the UIE. The effect of uneven illumination due to artificial light in the underwater images was corrected by combing the retinex theory with self guidance network (UIALN) [74].

The texture details of the underwater image were restored precisely by contrastive learning in which the U-Net architecture was modified with the proposed deformable convolutional residual block [75]. Multidimensional feature fusion and suppressing the unimportant features by an adaptive network [76] in which dewater pooling was used for highlighting the salient features. The GAN was employed to generate multi degradation model using models proposed in [24] and [25] to generate paired images [77] for restoration of underwater images. The CycleGAN was employed for generating underwater images using underwater degradation

model (UW-CycleGAN) [78]. A U-shape transformer [79] was proposed in which channel wise feature fusion and global feature fusion modules were specially designed for underwater image enhancement. A super lightweight three level neural network called Boths [80] was proposed for UIE.

A semantic attention guided network named SGUIE-Net [81] to restore degradations for the enhancement of underwater images. The removal of domain gap occurred between synthetic training images and underwater images by adaptive learning domain framework [42]. The attention based network named SCAUIE-Net [82] for extracting channel and spatial information from white balanced version of underwater images obtained from [32] for UIE. UIE-GAN [83] was proposed with two attention modules for extracting the spatial and channel features to enhance the degraded underwater images. UIE-FSMC [84] frame work was proposed by implementing the supervised learning using features corresponding datasets and the unsupervised learning using features from non-corresponding datasets followed by the color balance and contrast enhancement for the UIE. Adaptive feature fusion-based network named UIESC [85] with self-attention and contrastive learning for the UIE.

In the previous related works, the researchers worked with an assumption of equal rate of attenuation of both green and blue color components in underwater medium. So, they followed the same assumption for color correction to compensate the weak red color channel in accordance with the green color channel. But the color corrections based on the green color is not effective to overcome color dominancy because the results are affected by color artefacts. Further, the image quality improvement techniques based on the physical model are also not effective. We confide in the fact that possessing a longer wavelength, the red color losses its energy quickly due to absorption only in normal water. In polluted water, the green and or the blue colors get absorbed quickly compared to red. Hence, we infer that the image color distortion depends on the position of the camera, the depth of the underwater medium, the properties of the water and lighting conditions. The physical model based enhancement works even with color correction have the limitations of color casts. The model free works have the limitation of color artefacts. Due to lack of sufficient datasets of underwater images with real underwater scene and corresponding ground truth for different water types, the DL based image quality enhancement techniques are not effective to overcome the vision problems. Also, the DL based works are affected with color shades. Hence, a new enhancement technique is needed for improving the quality of degraded images captured in underwater medium. The main contributions of this work are:

(i) This work classifies the underwater images subjectively (based on visual perception) into five major types such as hazy, blue, green, bluish green and greenish blue color images and two special types such as yellow and dark underwater images.
(ii) It provides a comprehensive statistical analysis of benchmark underwater image datasets such as UIEB [50], RUIE [51] and SQUID [52] constituting more than 1000 images. The statistical conditions for the objective classification of five major types of underwater images are framed.
(iii) This work introduces a new color correction method based on the estimated value of the attenuation disparity between color channels.

III. STATISTICAL ANALYSIS OF UNDERWATER IMAGES

In the literature, some researchers attempted to enhance the underwater images based on image statistics [22], [29], [32], [33], [34], [86]. However, such methods used the image statistics only for obtaining mean pixel intensity, maximum and minimum values of pixel intensity for the color constancy. But in this work, the image statistics is used for classification of underwater images and correction of attenuation disparity occurred between color channels to preprocess the weak color channels to compensate the color imbalance. Let $I(x)$ be the captured underwater RGB image of size $m \times n$ where x represents the spatial coordinates (r, s) in 2-dimensional space. The image can be represented as [53]:

$$I(x) = (I^R(x), I^G(x), I^B(x)) \tag{4}$$

where $I^R(x), I^G(x)$ and $I^B(x)$ represent the three channels of RGB image respectively red, green and blue. The mean pixel intensity values of the color channels are estimated by

$$\begin{aligned} I_a^R &= \frac{1}{m \times n} \times \sum_{r=1}^{m} \sum_{s=1}^{n} I^R(r, s) \\ I_a^G &= \frac{1}{m \times n} \times \sum_{r=1}^{m} \sum_{s=1}^{n} I^G(r, s) \\ I_a^B &= \frac{1}{m \times n} \times \sum_{r=1}^{m} \sum_{s=1}^{n} I^B(r, s) \end{aligned} \tag{5}$$

where I_a^R, I_a^G and I_a^B are the mean pixel intensity of RGB color channels respectively. Based on the visual perception, ten images from each class of underwater images from UIEB, RUIE and SQUID datasets and haze images captured in air medium [10] are shown in Fig. 1 for presentation. The values of statistical analysis of images in Fig. 1 are shown in Table 1. Based on the mean pixel intensity of each color channels (RGB) and color of appearance without considering any conditions, the underwater images are classified roughly into five major types: 1) underwater haze image, 2) underwater greenish color image 3) underwater bluish color image, 4) underwater bluish-green color image and 5) underwater greenish-blue color image and two special types 1) yellowish image and 2) dark image. If there is no significant difference in the mean pixel intensity of any two color channels, then the image may be a haze image. The underwater images having similar pattern of attenuation of color channels like atmospheric haze images (i.e., all the color channels are attenuated almost equally) are categorized as underwater haze images. If the significant difference occurs in the mean pixel intensity between green color channel and both red and blue, then the green channel is the predominant one. In the same way, the

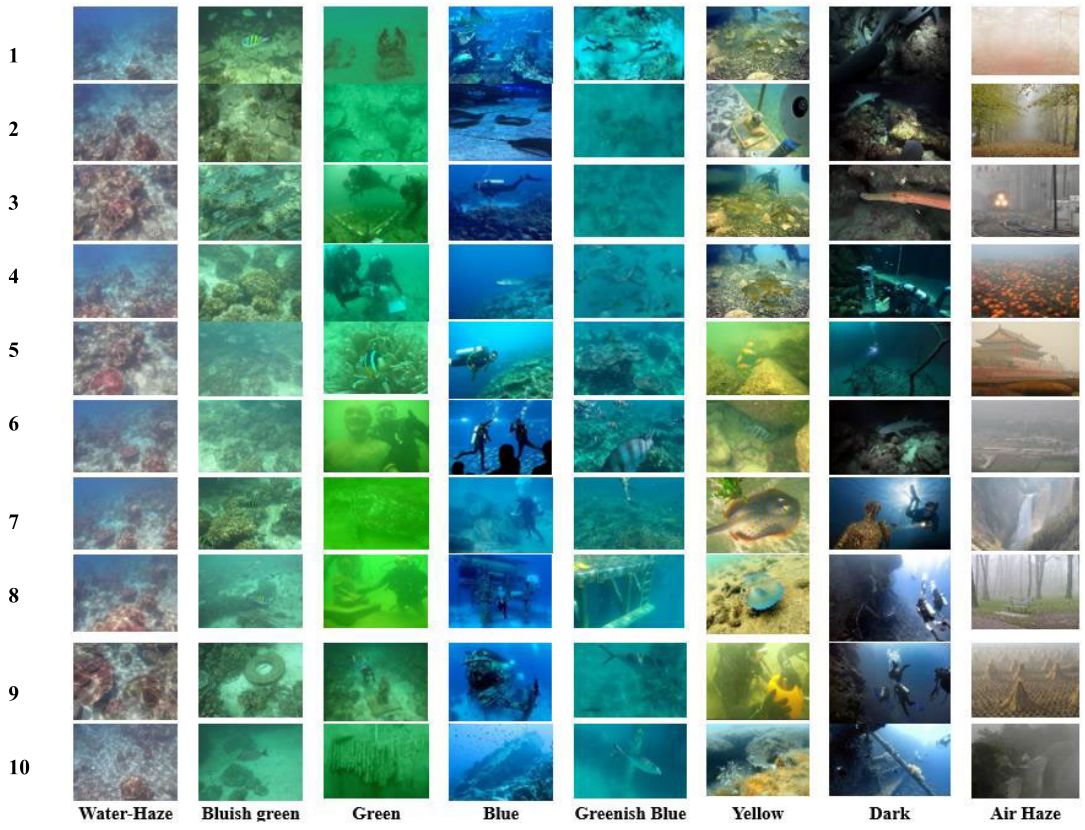

FIGURE 1. Images from UIEB Dataset and air-hazy images for statistical analysis.

TABLE 1. Average values of pixel intensity of color channels of images as in Fig.1.

Underwater Haze image				*Bluish-green color Image*			*Greenish color image*			*Yellowish color Image*		
Image	I_a^R	I_a^G	I_a^B	I_a^R	I_a^G	I_a^B	I_a^R	I_a^G	I_a^B	I_a^R	I_a^G	I_a^B
1	104.66	117.02	114.08	83.42	135.84	97.16	37.21	149.83	98.89	105.09	128.25	111.41
2	117.88	131.59	142.78	95.68	130.92	90.46	12.28	176.96	104.32	122.80	152.72	134.47
3	111.35	134.99	153.68	83.86	145.56	114.15	26.30	146.20	74.31	108.59	136.79	101.87
4	112.72	132.59	149.45	36.59	61.48	42.34	10.93	152.37	113.69	108.82	137.69	125.73
5	139.65	139.53	142.46	94.72	163.65	144.02	53.69	171.18	103.66	139.16	173.69	76.27
6	109.28	135.38	158.62	97.17	163.67	134.77	64.86	172.29	56.91	118.08	138.64	79.07
7	136.01	132.06	132.82	81.92	135.82	99.56	34.68	180.57	13.24	148.08	150.23	97.33
8	111.76	127.17	141.35	79.39	162.51	137.70	49.60	189.71	36.42	166.28	175.82	113.09
9	90.71	129.62	162.60	81.81	144.68	109.49	44.73	129.11	78.89	123.01	145.17	122.53
10	124.59	135.41	144.83	55.85	150.49	116.98	26.11	141.19	63.75	139.24	150.41	66.79
Mean	**115.86**	**131.54**	**144.27**	**79.04**	**139.46**	**108.66**	**36.04**	**160.94**	**74.41**	**127.92**	**148.94**	**102.86**
Image	*Bluish color image*			*Greenish blue color image*			*Dark Image*			*Atmospheric Haze Image*		
1	29.70	112.69	190.09	7.21	164.83	171.67	35.95	43.72	44.05	200.63	220.79	185.29
2	31.66	96.81	156.67	0.99	134.91	136.59	40.83	42.99	38.86	133.49	127.06	94.75
3	11.31	69.88	139.54	1.01	130.86	134.29	66.92	65.01	57.79	134.10	131.38	128.95
4	2.19	115.44	178.57	3.48	134.61	150.36	10.56	49.26	53.65	151.59	131.51	120.38
5	11.31	69.88	139.54	10.14	122.27	132.04	7.42	67.56	75.43	115.36	140.53	162.64
6	8.52	88.84	148.39	15.54	117.57	126.13	28.48	36.59	33.83	145.37	145.64	143.03
7	5.33	136.89	182.20	11.51	122.77	128.68	61.72	88.80	106.30	148.54	152.66	155.38
8	4.01	85.35	165.15	24.31	137.44	141.54	84.55	99.88	123.95	159.79	160.22	152.97
9	4.27	98.96	168.17	1.66	126.46	127.22	53.16	74.12	94.96	138.81	127.91	111.51
10	34.78	137.31	195.75	1.56	118.94	134.74	72.87	107.23	134.71	90.18	91.48	84.69
Mean	**14.31**	**101.21**	**166.41**	**7.74**	**131.07**	**138.33**	**46.25**	**67.52**	**76.35**	**141.79**	**142.92**	**133.96**

difference occurs between blue and both red and green, then the blue color is the predominant channel.

If the difference happens only between green and red, then the image appears in bluish green color. If the difference

TABLE 2. Inferences on statistics of underwater images and air haze images.

Type of image		Attenuation Color Channel (level)		
		Scattering	Absorption	Both
Underwater	Haze	Blue (low)	All R-G-B (low)	-
	Blue	Blue (high)	Red (moderate)	Green
	Green	Green (high)	Blue/ Red (low)	Red /Blue
	Bluish green	Blue (high)	Red (low)	Green
	Greenish Blue	Green (high)	Red (moderate)	Blue
	Yellow	Red/Green	Blue (moderate)	-
	Dark	-	Red	Green/Blue
Terrestrial Haze		Red (low)	Blue (high)	Green

occurs only between blue and red then the image looks in greenish blue color. The values depicted in Table 1 confirm the nonuniform attenuation of light in the underwater medium i.e., all the underwater images do not have similar attenuation pattern and hence the image formation model of terrestrial haze image is not effective for dehazing the underwater images. Further, the level of attenuation of all the color channels based on mean pixel intensity values is depicted in Table 2. Fig. 2 shows different appearances of underwater images and air haze image with the concerned monochromatic color channel (Red, Green and Blue) images. Based on the visual perception of the images shown in Fig. 2 along with values in Table 1, it is inferred that the color of appearance of underwater images depends on the mean pixel intensity of color channels.

Hence the underwater images can be objectively classified based on image statistics by considering the following facts:

1.The statistical analysis of terrestrial haze images shows that the maximum and minimum values of pixel intensity of all planes in RGB space do not undergo the intensity jumps. Also, such haze images occurred due to the presence of haze, smoke and fog with different concentrations of tiny particles present in the lower atmosphere. Typically, haze causes the obscuration of the scene, subject to the density of haze. But in the context of underwater images, such statistics are entirely different since the intensity jump occurs in the pixel intensity of color channels due to the absorption of light. This indicates the loss of energy followed by wavelength shifting from long to short and thus the red color light shifts either to green or blue or in the range of blue-green. The jump in pixel intensity is due also to the two degrading factors of underwater medium – i) depth of the target scene from the surface of water and ii) properties of water medium (saline or pure or turbid) which may have transparency but contains dissolved components with suspended particles.

2. We rely on the fact that in underwater medium, the predominant color of the traversing light (almost blue and sometimes green) attenuates only due to scattering whereas the highly degraded color component (almost red in the case of the bluish color image and sometimes blue in case of greenish image) attenuates only due to absorption. The red color component in the case of a greenish color image or the green component in the case of a bluish color image degrades moderately due to both scattering and absorption.

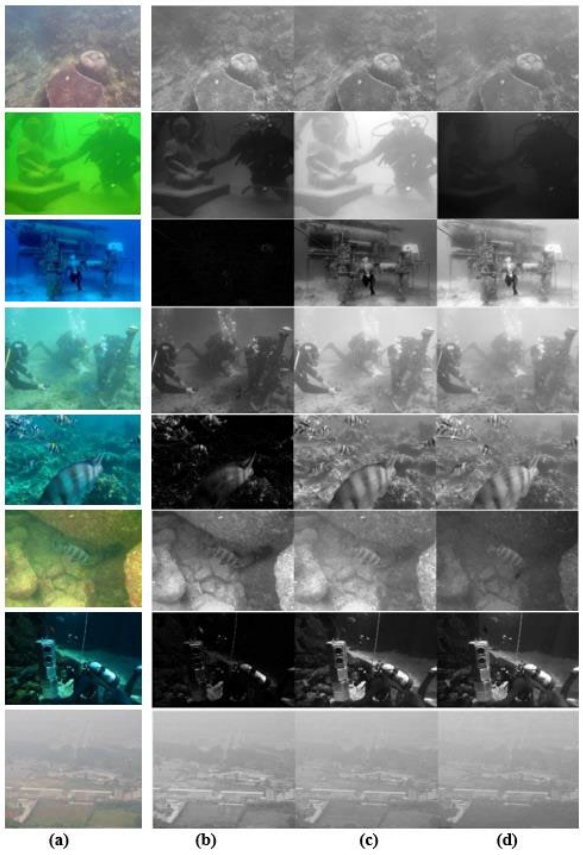

FIGURE 2. Color channel (monochromatic) images of underwater images. a) original image, b) red channel image c) green channel image and d) blue channel image.

3. Further, the GW [53] assumption method removes the color tone that causes the appearance of the image in bluish color. But in selective absorption, the mean pixel intensity of the red color channel is very low for blue, bluish green and greenish blue images and hence the GW grieves from red artefacts severely. In greenish images, the mean pixel intensity for both red and blue color images is low. In these two cases, there is a significant difference between the mean pixel intensity of color channels. The results of the conventional color constancy [37] methods such as GW theory [54], shades of Grey [36], Gray Edge [38], max-RGB [35], [39] and color equalization [55] suffer from unwanted red artefacts at pixel locations where green and blue color channels have significant pixel intensity whereas the red does not. Hence, it is impossible to enhance all the underwater images by a color correction algorithm. But it may be possible for image classification based color correction in a single method. As discussed earlier, the classification of underwater images is introduced using image statistics based on the pattern of attenuation of color channels (as shown in Fig. 2) and the rate of attenuation due to absorption of light. The in-depth analysis of Table 2 shows that the color channels of underwater images are degraded in five types of attenuation

patterns which help to classify the images into five types as in Table 3. The intensity of pixels of an image captured in a medium is directly proportional to the energy of traversing light in that medium [36]. The absorption may be selective or conditional depending upon the depth of the target scene from the surface of the water and the biological conditions of the water medium.

IV. CLASSIFICATION OF UNDERWATER IMAGES

A. ESTIMATION OF RATE OF ATTENUATION OF COLOR CHANNELS OF UNDERWATER IMAGES

With respect to the predominant color component of an underwater image, the total attenuation, rate of loss of information and rate of information carried out by each color component for the five classes of underwater images are estimated from the statistical observations. The total rate of attenuation of light (ρ^T) is defined as the ratio of the average of mean pixel intensity of the three color channels (RGB) to the maximum pixel intensity of the type of image representation in bits and it is given by

$$\rho^T = \frac{\sum_c \sum_y \sum_x f^c(x,y)}{(3 \times m \times n \times (L-1))} \tag{6}$$

and $0 \leq f(x,y) \geq L-1$ and $L = 2^n$. Where f is the captured image having a dimension of m rows and n columns with pixel location x and y, $c \in \{red, green, blue\}$ is the concerned color channel, n is the number of bits for image representation (usually n =8 i.e., $L = 256$) and $0 \leq \rho^T \leq 1$. If $\rho^T = 0$ then it implies that the light losses its energy completely due to attenuation and the received pixel intensity is zero. If $\rho^T = 1$ then it represents that there is no loss of energy and the pixel intensity is $L-1$. Through this, it is clear that the light does not attenuate whenever the pixel intensity is $L-1$ and the light attenuates completely if the pixel intensity is zero. If the pixel intensity is greater than zero and less than $L-1$, then the received light ray is attenuated but not completely while traversing through the medium. Also, it is easy to estimate the rate of attenuation of individual light color from the pixel intensity of the captured image. The rate of attenuation of light color (ρ^c) is given by

$$\rho^c = \frac{\sum_y \sum_x f^c(x,y)}{(m \times n \times (L-1))} \tag{7}$$

To compensate the attenuation, it is necessary to estimate the rate of attenuation of the degraded color channel(s) with respect to the predominant color channel. The rate of attenuation of red color with respect to blue can be estimated from the ratio of the total attenuation of the red channel to the total attenuation of the blue channel $(\rho^{rb}) = \left(\frac{\rho^R}{\rho^B}\right)$. Similarly for other color channels, $\rho^{rg} = \left(\frac{\rho^R}{\rho^G}\right)$, $\rho^{gb} = \left(\frac{\rho^G}{\rho^B}\right)$, $\rho^{gr} = \left(\frac{\rho^G}{\rho^R}\right)$, $\rho^{br} = \left(\frac{\rho^B}{\rho^R}\right)$ and $\rho^{bg} = \left(\frac{\rho^B}{\rho^G}\right)$. For, approximation, the rate of attenuation due to absorption (α) in terms of pixel intensity is considered as the ratio of the mean of average pixel intensity (μ) of highly degraded color channel image to the μ of predominant color channel image of any dataset contains more than 1000 images as provided in Table 1. Then the optical model, equation (1) is modified using the estimated values to represent the underwater image since the camera system is same but only the medium is different.

TABLE 3. Estimated attenuation values of underwater images and air haze images.

Type of image		Attenuation			
		ρ^T	ρ^R	ρ^G	ρ^B
Underwater	Haze	0.5119	0.4544	0.5158	0.5658
	Blue	0.3685	0.0561	0.3969	0.6526
	Green	0.3548	0.1413	0.6311	0.2918
	Bluish green	0.4277	0.3099	0.5469	0.4261
	Greenish Blue	0.2054	0.0304	0.5140	0.5425
	Yellow	0.4964	0.5016	0.5841	0.4034
	Dark	0.2485	0.1814	0.2648	0.2994
Terrestrial Haze		0.5473	0.5560	0.5605	0.5253

B. STATISTICAL CONDITIONS FOR CLASSIFICATION OF UNDERWATER IMAGES

Based on the mean pixel intensity of the color channels of RGB images, the brightest pixels spotted in the color channel and the rate of attenuation the underwater images are classified with the following statistical conditions.

1. Underwater haze image

$$I_a^B > I_a^G > I_a^R \; and \; I_a^R \geq 0.7\left(I_a^G\right) \geq 0.7\left(I_a^B\right)$$
$$min(I^B(x)) > min(I^G(x)) > min(I^R(x))$$
$$max(I^B(x)) = max(I^G(x)) = max(I^R(x))$$

where $(L-1) \leq max(I^c(x)) \geq min(I^c(x)) \geq 0$ in the dynamic range of pixel intensity of color channels.

2. Underwater bluish color image

$$I_a^B > I_a^G \text{ and } 0.2I_a^G \geq I_a^R \leq 0.4(I_a^B)$$
$$\min(I^B(x)) > \min(I^G(x)) > \min(I^R(x))$$
$$\max(I^B(x)) > \max(I^G(x)) > \max(I^R(x))$$

3. Underwater greenish color image

$$I_a^G > I_a^R \text{ and } I_a^B \leq 0.4(I_a^G)$$
$$\min(I^G(x)) > \min(I^R(x)) > \min(I^B(x))$$
$$\max(I^G(x)) > \max(I^R(x)) > \max(I^B(x))$$

4. Underwater greenish-blue color

$$I_a^B > I_a^G > I_a^R \text{ and } I_a^G \geq 0.5(I_a^B)$$
$$\min(I^B(x)) > \min(I^G(x)) > \min(I^R(x))$$
$$\max(I^B(x)) = \max(I^G(x)) = \max(I^R(x))$$

5. Underwater bluish-green color

$$I_a^G > I_a^B > I_a^R \text{ and } I_a^B \geq 0.5(I_a^G)$$
$$\min(I^B(x)) > \min(I^G(x)) > \min(I^R(x))$$
$$\max(I^G(x)) = \max(I^B(x)) > \max(I^R(x))$$

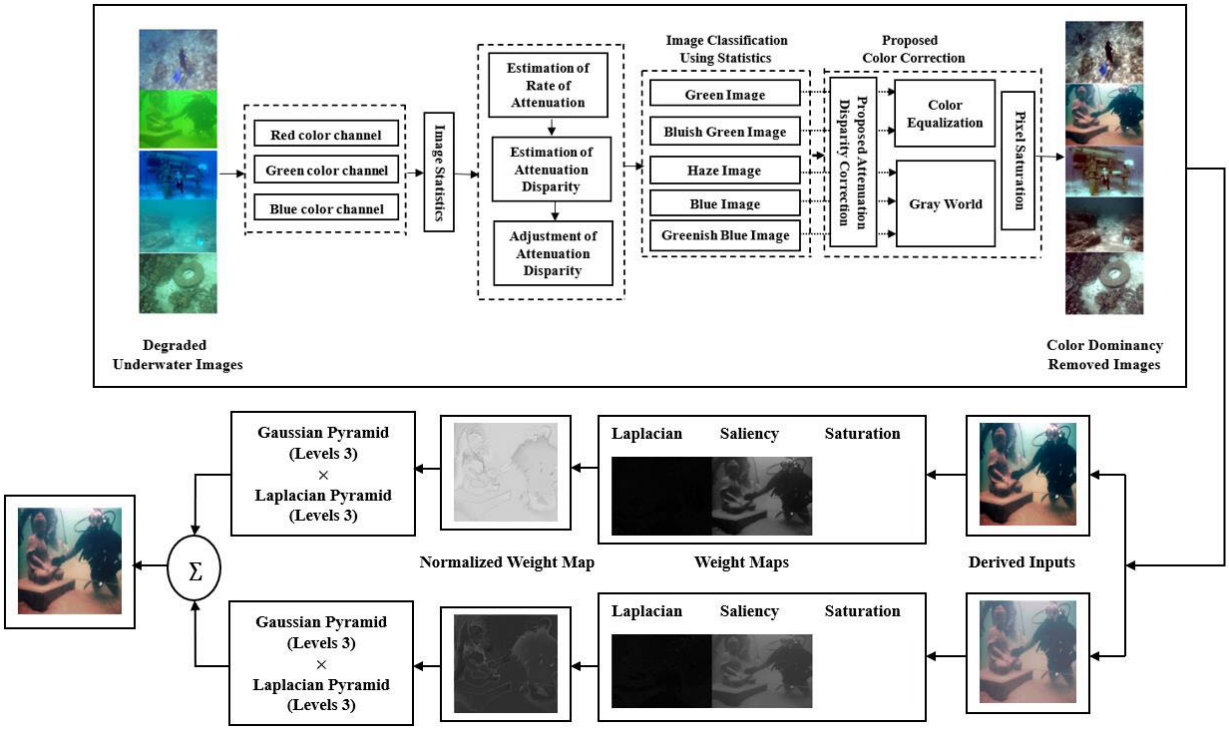

FIGURE 3. Flow chart of proposed method.

Based on the rate of attenuation of light estimated from the captured underwater images using image statistics and the conditions for the classification underwater images, we can modify the equation s (1) and (2) for restoring the underwater images. But in this article, the statistical analysis of images is used only for the confirmation of our assumption for the proposed color correction.

V. PROPOSED METHODOLOGY

The proposed methodology involves two stages namely a) Color Correction and b) Multiscale image fusion. The first stage aims to compensate for the color distortion whereas the second stage compensates the losses due to scattering.

A. COLOR CORRECTION

The overall procedures of the proposed method are depicted in Fig. 3. The adjustment of attenuation disparity between degraded color channels and the predominant color channel can restore the information of the degraded color channel. We observe that more than 40 percent of red pixels have zero intensity value in bluish, greenish-blue and bluish-green color images. Also, the remaining 60 percent of pixels have very less intensity compared to green and blue color channels. As the Gray-World assumption method is applicable for homogeneous air medium, it is not suitable to enhance the underwater images. So, we perform a global pointwise pre-correction to the degraded color channels to increase the very low pixel intensity of highly attenuated color channels. For this, the following equations (8) to (10) are proposed as a pre-color correction step before employing the Gray-World assumption for underwater haze, blue and greenish blue color images and color equalization technique for green and bluish green color images.

$$I^{rc}(x) = I^{R}(x) + D_r(x) \tag{8}$$

$$I^{gc}(x) = I^{G}(x) + D_g(x) \tag{9}$$

$$I^{bc}(x) = I^{B}(x) + D_b(x) \tag{10}$$

In the case of underwater haze images, we apply the equation (8) or (9) for pre-correcting the red or green color channel. Fig.4 depicts the results of the proposed color balancing. The proposed color correction increases the pixel intensity of weak color channels from very low value to high value and thus the appearance of the particular color channel is turned from black color to gray with some scene information. Thereafter, the GW or the color equalization is employed to shift both the high pixel intensity value (white) and low pixel intensity value (black) to the middle pixel intensity value (gray) and thus, the appearance of pre-corrected weak color channel turns from white to gray with low scene information. Then the conventional pixel saturation technique is employed for saturating the 1% bottom pixels and 1% top pixels to adjust the distribution of the pixel intensity for recovering the scene information for the improvement of image contrast. Fig. 4 (i) (a) is the original bluish underwater image and Fig. 4 (i) (b) is the greenish underwater image with corresponding RGB histogram.

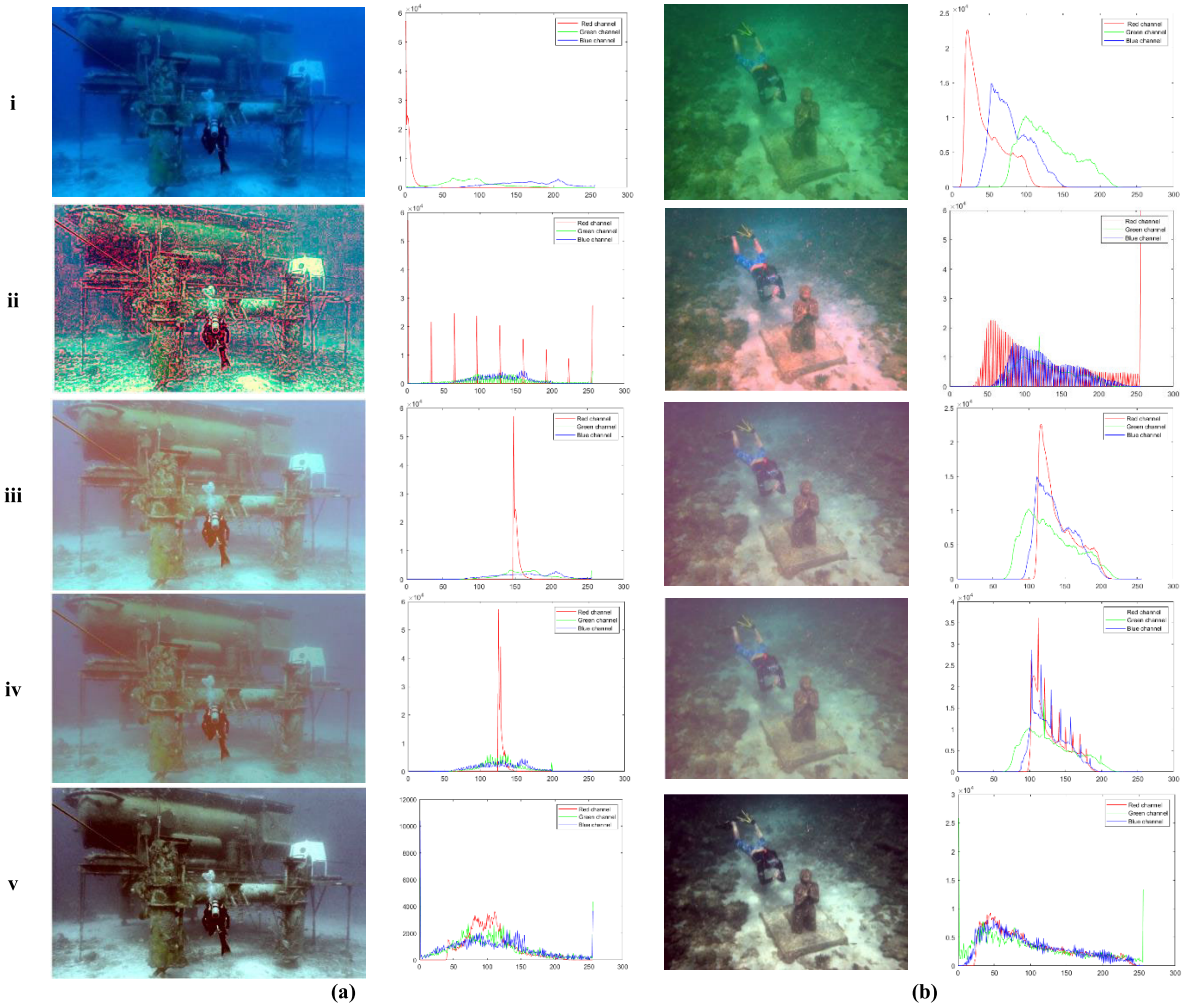

FIGURE 4. Results of the proposed method. i) original underwater image, ii) Results of Gray World Method, iii) Result of proposed disparity correction, iv) result of DC+GW, v) result of GW+DC+IA. (a) Blue image with RGB-Histogram and (b) Green image with RGB-Histogram.

The histogram component of red channel of blue image lies at the left side (nearly zero) and blue channel at the right side which indicates the deteriorated red and dominated blue. In the histogram of greenish image, the green channel lies right side and the red channel lies between zero to middle level and the blue channel lies in the middle and this indicates that the green dominancy. Fig. 4(ii) is the GW version of original underwater image. The GW version of bluish image has red artefacts whereas the GW version of greenish image has red shades due to over compensation of red channel. Fig. 4 (iii) is the proposed disparity corrected (DC) version of original underwater image.

In the components of RGB histogram of DC version of both bluish and greenish images, all the three channels are equally distributed in the middle which represents no color dominancy. However, the DC version looks hazy image and over white balanced without color dominancy. Fig. 4(iv) is the resultant image of combined DC and GW version of bluish image and DC and CE version of greenish image. The components of RGB histogram are evenly distributed in the middle for both bluish and greenish images which indicates the appropriate white balancing but images are still hazy. Fig. 4(v) is the resultant image of DC, GW (for blue image) or CE (for green image) and image adjustment (IA) by saturation of top and bottom 1%-pixel intensity levels. The RGB histogram components of all the three color channels in Fig. 4(v) are distribute from lower to higher pixel intensity levels evenly and this indicates the good image quality. The GW always results with the red artefacts/shades for the images captured in non-homogeneous medium. The proposed color channel attenuation correction method plays a vital role in color constancy as a preprocessing to GW and CE methods.

B. MULTISCALE IMAGE FUSION

To improve the quality of color manipulated images obtained from the proposed color correction, the multiscale fusion used by Ancuti et al. [32] and Wang et al. [92] is employed. The too brightness in the color corrected version is balanced using

Gamma Correction. The gamma corrected and the sharpened images are blended using weighted image fusion technique. The gamma correction of image luminance (L^* plane of $L^*a^*b^*$ model), $L^{\delta}(x)$ (power law version) is,

$$L^{\delta}(x) = \vartheta \times L^{M}(x)^{\gamma}, 0 \leq \gamma \leq \infty \text{ and } 0 \leq \vartheta \leq 1 \quad (11)$$

where, ϑ is a constant which maps the input and the output values of the transformation to lie in the range of 0 to 1 and γ is a positive power factor. The contrast of the image is improved by varying the values of γ and ϑ. For appropriate correction, the best value of γ is 0.7 obtained and $\vartheta = 1$. If $\gamma > 0.7$, the image is bleached out whereas if $\gamma < 0.7$, the image is dark.

Due to this intensity correction, there is a loss of information occurs either at under exposed or over exposed parts. Hence, a sharpened version of the color corrected is obtained using unsharp masking (UM). The UM is employed to sharpen the luminance of the image. The difference between the original image and its smoothed version is the sharpened version. First, the mask, $L^{mask}(x)$ is obtained by estimating the difference between the original luminance, $L^{M}(x)$ band its blurred version, $\overline{L^{M}(x)}$. Then the sharpened version of the luminance, $L^{sharp}(x)$ is obtained by adding the masked luminance with the original luminance.

$$L^{mask}(x) = L^{M}(x) - \overline{L^{M}(x)}$$
$$L^{sharp}(x) = L^{M}(x) - L^{mask}(x)$$

In general, high values are assigned to texture and edges of an image by Laplacian filter which provides global contrast. The absolute value of the Laplacian filtered form of luminance of color corrected image is estimated and considered it as edge map $\left(L^{j}_{lf}\right)$. The low pass filter provides local contrast information and hence it is used to estimate the concerned weight map for the image local contrast $\left(L^{j}_{lpf}\right)$. It is estimated as the absolute value of the difference between the luminance of original image and its low pass version.

$$L^{j}_{lpf} = \left\| i^{j}_{o} - i^{j}_{lp} \right\| \quad (12)$$

where i^{j}_{o} is the luminance of the j^{th} input $\{j = 1, 2\}$ and i^{j}_{lp} is the low pass version of i^{j}_{o}. The filtering of i^{j}_{o} with a kernel of $\left[2^{-4}, 2^{-2}, 3{\times}2^{-3}, 2^{-2}, 2^{-4}\right]$ and cut off frequency of low pass is 1.14182 provides the i^{j}_{lp}.

The weight of saliency map (S_{wm}) is estimated as

$$L^{j}_{sm} = \left(L - L_{\mu}\right)^2 + \left(a - a_{\mu}\right)^2 + \left(b - b_{\mu}\right)^2 \quad (13)$$

where L_{μ} is the mean of luminance channel and a_{μ} and b_{μ} are the mean value of color channels a^* and b^* channels respectively. The degree of exposure of pixels (L_{em}) increases the exactness of the blended image. The weight map of L_{em} is given by

$$L^{j}_{em}(s,t) = \exp\left(\frac{\left(-\left(I^{j}(s,t) - 0.5\right)^2\right)}{2{\times}\sigma^2}\right) \quad (14)$$

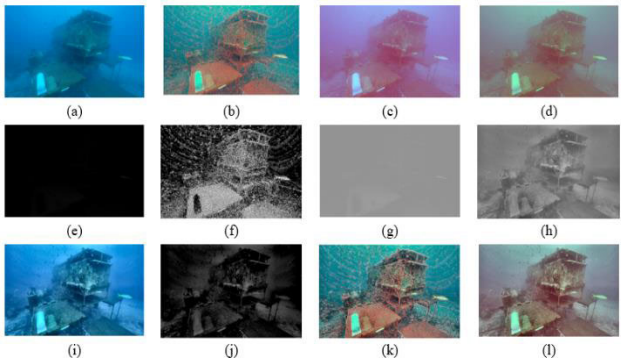

FIGURE 5. Comparative Analysis of images. a) and e) original image and its red channel image, b) and f) Gray World (GW) and its red channel, c) and g) attenuation adjustment and its red channel, d) and h) Attenuation adjustment + GW and its red channel, i) and j) CLAHE and its red channel, k) GW + CLAHE, l) final result of the proposed method of attenuation adjustment + GW + CLAHE.

where $I^{j}(s,t)$ is the intensity of concerned j^{th} derived input image at the pixel location of (s,t) and $\sigma = 0.25$. The weights are normalized to obtain normalized map $\left(N^{j}_{wm}\right)$. With the help of N^{j}_{wm}, the consistent result is obtained such that the overall sum of all weight maps is 1 at every pixel location.

$$N^{1}_{wm} = \frac{L^{1}_{lf} + L^{1}_{lpf} + L^{1}_{sm} + L^{1}_{em}}{\sum_j \left(L^{j}_{lf} + L^{j}_{lpf} + L^{j}_{sm} + L^{j}_{em}\right)}$$
$$N^{2}_{wm} = \frac{L^{2}_{gwm} + L^{2}_{lwm} + L^{2}_{sm} + L^{2}_{em}}{\sum_j \left(L^{j}_{lf} + L^{j}_{lpf} + L^{j}_{sm} + L^{j}_{em}\right)} \quad (15)$$

Finally, 3-level Gaussian and Laplacian operators are employed for convolving the two derived images using the kernel of $\left[2^{-4}, 2^{-2}, 3{\times}2^{-3}, 2^{-2}, 2^{-4}\right]$. The final enhanced image, $J(s,t)$ is obtained by summing of output of 3-level pyramidal convolutions of the two derived images by

$$J(s,t) = \sum_{j=1}^{2} \sum_{k=1}^{3} g^{k}\left\{N^{j}_{wm}\right\} \times l^{k}\left\{G^{M}(x)\right\} \quad (16)$$

where $k = 3$ represents the pyramidal levels, $j = 2$ represents the derived images, $1\{.\}$ represents the Laplacian operator and $g\{.\}$ represents the Gaussian operator.

VI. RESULTS AND DISCUSSION

The proposed method is implemented using MATLAB R2020a version installed in a personal computer with configuration of i3 Intel 11th Generation Processor with 8GB RAM. The resultant image and its red component of GW, attenuation adjustment, Attenuation adjustment followed by GW, contrast limited adaptive histogram equalization (CLAHE) [38], GW followed by CLAHE and the proposed Attenuation Adjustment followed by GW and CLAHE are depicted in Fig. 4. The histogram representation of three (RGB) monochromatic images of five classes of original underwater images, the results of Ancuti et al and the proposed method are plotted in Fig. 5. Fig. 5(a) represents the histogram of three monochromatic color channels of original underwater

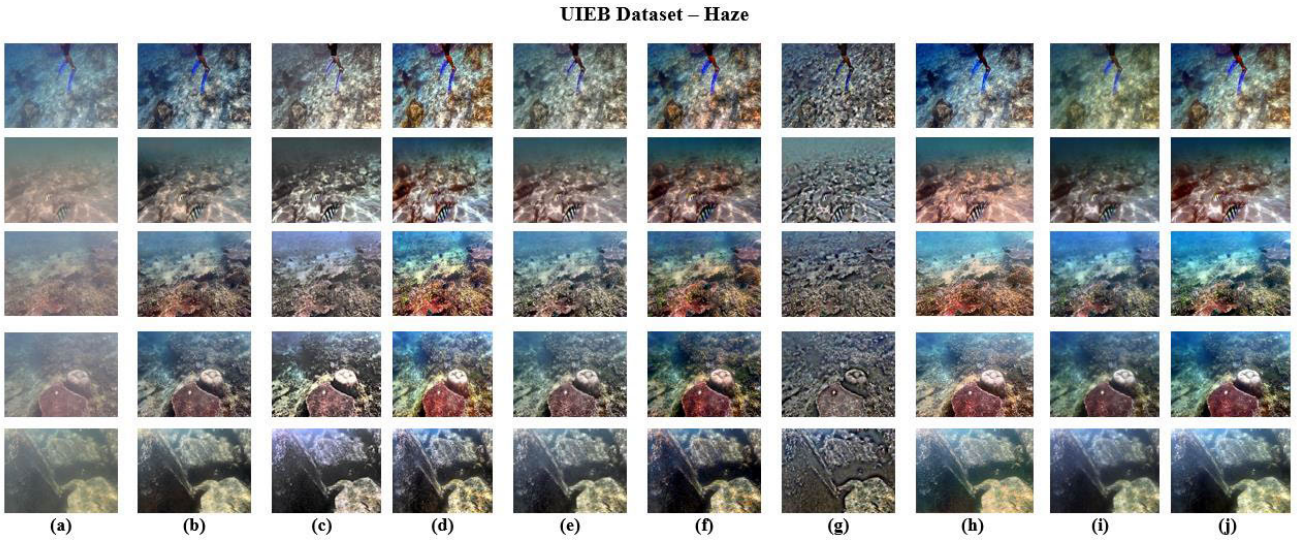

FIGURE 6. Results of Haze images. a) original image, b) TOPAL, c) PCDE, d) ACCE, e) MLLE, f) VCSE, g) TEBCF, h) SGUIE-Net, i) Color Mixing and j) Proposed Method.

images. The first row to the fifth row of Fig.5 respectively represents the combined histogram of red, green and blue color planes of underwater haze, green, blue, greenish blue and bluish green color images. In underwater haze images, the components of red, green and blue channels are all concentrated at the middle of the intensity scale and hence they have almost equal image information. But the histogram of the blue tone of the haze image is narrow compared to red which represents the low contrast. In the case of an underwater green image, the components of the histogram of red and blue channels are concentrated towards the dark (low intensity) side and the green channel is concentrated towards the light (high intensity) side and it represents the predominance of green color. The histogram of red and blue color is narrow compared to green and hence the red and blue channels do not carry significant information. In case of the blue color image, the components of red are concentrated towards the leftmost side (very dark) with a very narrow histogram which represents the channel least or no information whereas the components of blue and green have occupied the entire range of intensity scale. But the number of pixels of both green and blue with high intensity is very less and hence the image has less information even in the blue color channel.

For, the greenish blue image, the red components are concentrated towards the leftmost side with a very narrow histogram and the components of blue and green occupy the entire range with a green peak. In the case of bluish green image, all the red components are concentrated within the middle and the green and blue components are concentrated in the entire range. But the green component which is extended to high intensity values compared with the blue. In some cases, the red histogram may concentrate towards the leftmost side in the case of the bluish green image. Finally, it can be inferred that the pixels of all three color Finally, it can be inferred that the pixels of all three color channels do not occupy the entire range of intensity levels with non-uniform distribution of pixels. But for a high contrast image, the pixels lean towards occupying the entire range of intensity levels with uniform distribution of pixels. So, it is required to advance a function which transforms the low quality image into a high quality image based only on the information present in the histogram of the original underwater image.

The histogram of the enhanced images of Kumar and Bhandari [31] and the proposed method are shown in Fig. 5(b) and 5(c) respectively. Though the components of the histogram of the three color channels of Fig. 6(b) are distributed uniformly and exhibit a variety of gray tones, the image is suffered from a yellow shade due to the equal distribution of red and blue color components. On the other hand, it is required to convert the narrow histogram to wide, a wide histogram to nominal and non-uniform distribution of pixels to uniform distribution, in order to get a high quality image from a low quality image. The results of the proposed method in Fig. 6(c), shows that the pixels are distributed uniformly and the pixels also occupy the entire range of possible intensity levels without a narrow histogram. Also, the number of pixels whose intensity values are high have increased in all the color channels for all types of underwater images except green color images. In a green color image, the proposed method reduces the number of pixels in the green color channel whose intensity values are high and increased the number of pixels in red and blue color channels whose intensity is low. In case of a haze image, the histogram of all the color channels is wide with uniform distribution in the results of the proposed method. In case of blue and greenish blue images, the narrow red histogram is converted to a wide histogram in the proposed method. Hence, the results of the proposed method, the distribution of histogram components

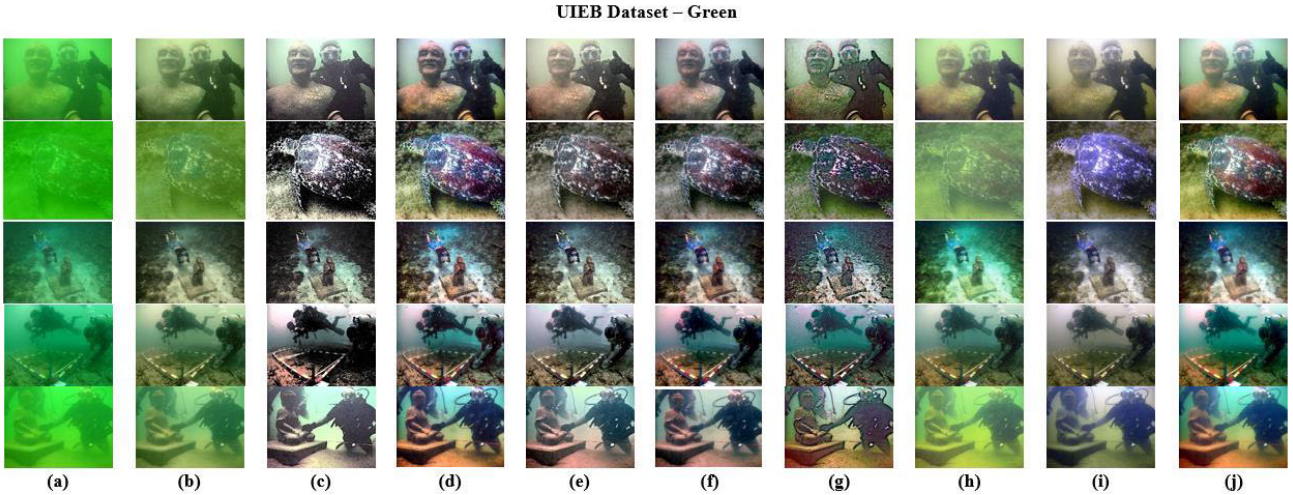

FIGURE 7. Results of Green images. a) original image, b) TOPAL, c) PCDE, d) ACCE, e) MLLE, f) VCSE, g) TEBCF, h) SGUIE-Net, i) Color Mixing and j) Proposed Method.

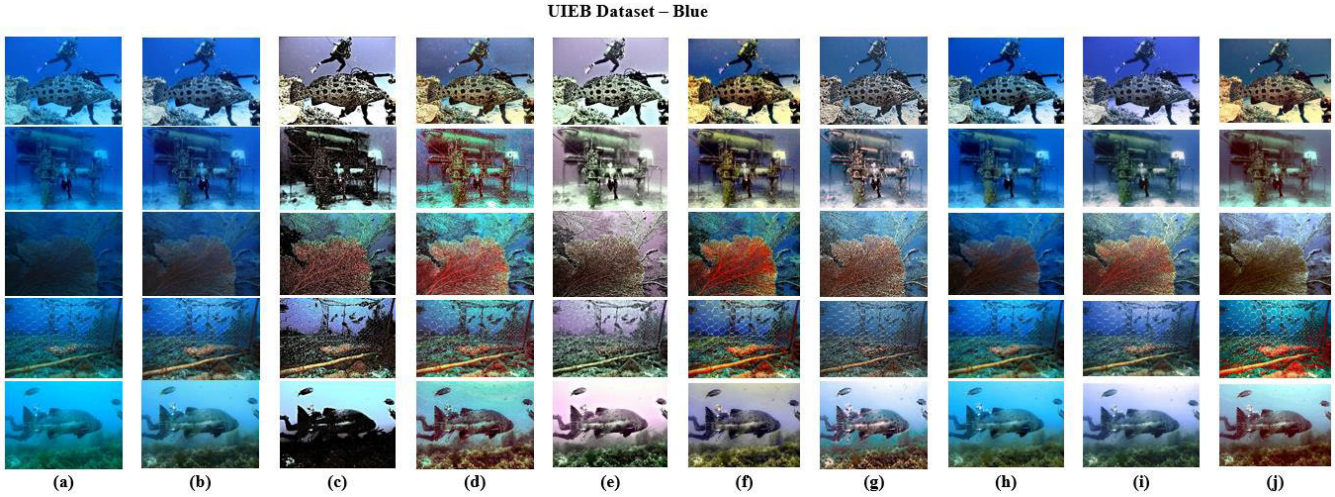

FIGURE 8. Results of blue images. a) original image, b) TOPAL, c) PCDE, d) ACCE, e) MLLE, f) VCSE, g) TEBCF, h) SGUIE-Net, i) Color mixing and j) Proposed method.

is uniform in the entire range of possible intensity levels and a minimum of gray tones and the net result is the enhanced image without any color shades.

A. QUALITATIVE ANALYSIS

The performance of the proposed method has been compared with the existing methods both quantitatively and qualitatively. The publicly available non-commercial code is used to obtain the results of the existing methods. The performance of the proposed method is compared with the results of Color Mixing [32], SGUIE-Net [49], MMLE [66], TOPAL [72], VCSE [87], TEBCF [88], PCDE [89] and ACCE [90]. Fig. 6, Fig. 7, Fig. 8, Fig. 9, Fig. 10 and Fig. 11 depict the results of Color Mixing [32], SGUIE-Net [49], MMLE [66], TOPAL [72], VCSE [87], TEBCF [88], PCDE [89] and ACCE [90] for the haze images, greenish images, bluish images, bluish green images, greenish blue images and yellow images respectively. The dark underwater images are not focused in this article. For underwater haze images, haze is not removed completely by TOPAL [72], MLLE [66], SGUIE-net [49]. Further, the methods TOPAL [72], TEBCF [88] and Color Mixing [32] result with dark background dark and thus the distant objects are not clearly visible. The methods such as ACCE [90], VCSE [87] and SGUIE-Net [49] remove the haze well but the red channel is over compensated. The method PCDE [89] results with over white balancing. The performance of TEBCF [88] is poor since the resultant images are severely affected by noise and the object identification is difficult due to over darkness. The proposed method removes the haze well and the image quality is improved substantially. In case of greenish images as in Fig. 7, TOPAL [72] and SGUIE-Net [49] do not remove

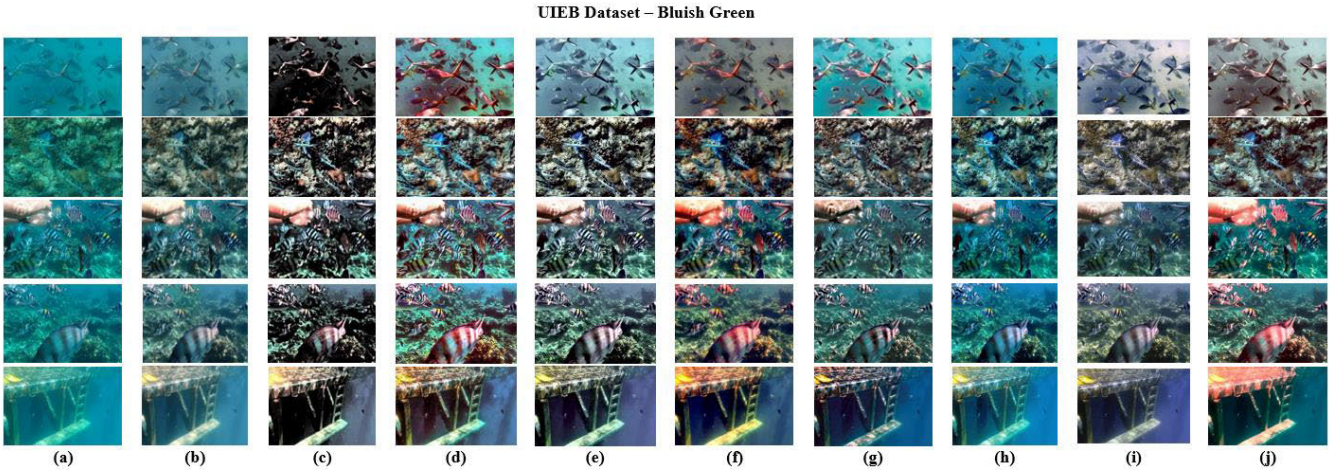

FIGURE 9. Results of bluish green images. a) original image, b) TOPAL, c) PCDE, d) ACCE, e) MLLE, f) VCSE, g) TEBCF, h) SGUIE-Net, i) Color Mixing and j) Proposed method.

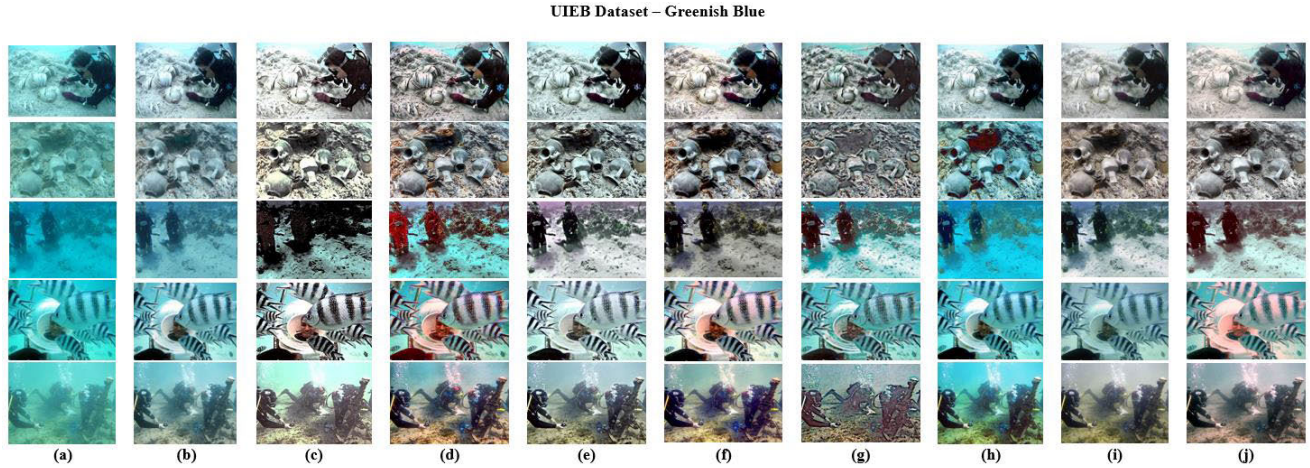

FIGURE 10. Results of greenish blue images. a) original image, b) TOPAL, c) PCDE, d) ACCE, e) MLLE, f) VCSE, g) TEBCF, h) SGUIE-Net, i) Color Mixing and j) Proposed Method.

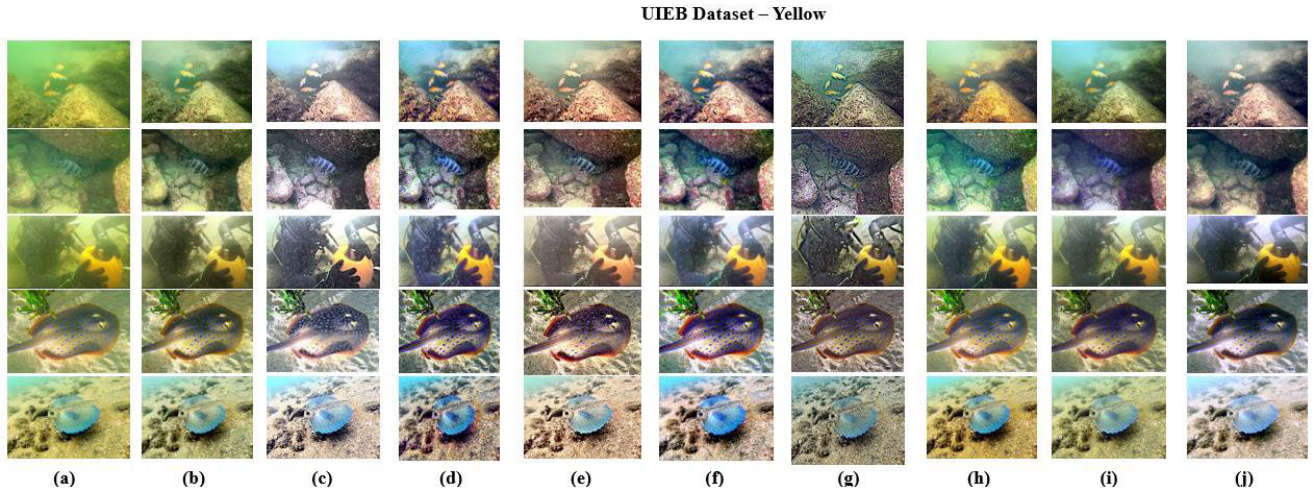

FIGURE 11. Results of Yellow images. a) original image, b) TOPAL, c) PCDE, d) ACCE, e) MLLE, f) VCSE, g) TEBCF, h) SGUIE-Net, i) Color Mixing and j) Proposed Method.

color dominancy. ACCE [90], MLLE [66] and VCSE [87] remove green color dominancy well but the red color is over compensated and hence the resultant images are affected with red artefacts or red shades. PCDE [89] results with over brightness in the foreground and darkness in the background.

The result of Color Mixing [32] for greenish images is quality improved version of original images but the drawback is the presence of yellow shades due to equal compensation of red with green. The performance of TEBCF [88] is poor since the results are affected with darkness. The proposed method achieves good color compensation in reducing the green dominancy but in some images where mean value of red is less than blue, the images are affected with some red shades.

For the bluish images as in Fig. 8. In the scenario of bluish underwater images, the methods TOPAL [72], TEBCF [88] and SGUIE-Net [49] do not remove the color dominancy in bluish images but the mean value of red color has increased. The overall performance of [49], [72], and [88] are poor. PCDE [89] removes the blue color dominancy but it results with image darkness. Although VCSE [87] reduces the blue dominancy, the red color is over compensated. When compared to existing methods, the proposed method reduces color dominancy in bluish images but in some cases where the red color has mean value of below ten, the results are affected with red artefacts. Color Mixing [32] removes blue dominancy in the foreground region only and the blue color dominancy is not removed in the background region in bluish images. ACCE [90] removes blue dominancy but the green color is over compensated.

From Fig. 9, TOPAL [72] and SGUIE-Net [49] do not remove the color dominancy completely for the bluish green images. However, the image quality is improved. Although the color dominancy has been removed by ACCE [90] and VCSE [87], the resultant images have red artefacts due to over compensation of red channel. PCDE [89] removes the color dominancy substantially but the resultant images are severely affected by image darkness. The resultant images of Color Mixing [32] do not have color dominancy but the background images are not clearly visible. MLLE [66] shows good performances in removing color dominancy as well as the image quality is also improved. TEBCF [88] shows poor performances in removing the color dominancy. The results of the proposed method reveal that it outperforms than existing methods in terms of color dominancy removal as well as contrast enhancement. Fig. 10 shows that TOPAL [72], TEBCF [88] and SGUIE-Net [49] are poorly performed for color removal of color dominancy in greenish blue images. ACCE [90] has the drawback of red artefacts. PCDE [89] is affected by over darkness. MLLE [66] shows good performances in removing color dominancy as well as the image quality is also improved. TEBCF [88] shows poor performances in removing the color dominancy.

In case of yellowish images as in Fig. 11, TOPAL and the proposed method improve the image quality but the result of TOPAL has the limitation of over brightness. The yellow shade is not completely removed by MLLE, SGUIE-Net and Color Mixing. The blue color is over compensated in ACCE and VCSE. TEBCF underperforms than other methods.

The results of the proposed method reveal that it outperforms than existing methods in terms of color dominancy removal as well as contrast enhancement. The contrast of the VCSE [87] is low but color dominancy has removed. MLLE [66] and Color Mixing [32] show better performance but they do not show the foreground regions such as shadows of divers clearly. The proposed method improves the image quality substantially when compared to existing methods.

B. QUANTITATIVE ANALYSIS

In the literature, the performances of the underwater image enhancement methods were measured by underwater color image quality evaluation (UCIQE) metrics [62] and underwater image quality measures (UIQM) [63]. UCIQE is a measure of weighted sum of contrast of luminance (L_c), standard deviation of chroma (σ) and average of saturation (λ_s) weighted with a, b and c respectively in the CIELab color plane. UCIQE is estimated by

$$\text{UCIQE} = a \times L_c + b \times \sigma + c \times \lambda_c \tag{17}$$

The authors in [62] considered the degradation of underwater images by marine snow, image blurring and color casts. With the help of an image dataset of selective 44 degraded underwater images to optimize the values of a, b and c such that their sum is always 1, the authors consider $a = 0.4680$, $b = 0.2576$ and $c = 0.2745$.

Also, these values are not appropriate to all other underwater images taken in different environment. However, we consider the same values of a, b and c as in [62] to measure the UCIQE. The UIQM [63] is a measure of weighted sum of colorfulness (CF) measured in HSV color space, contrast measure (CM) in RGB space and image sharpness (IS) weighted with a, b and c respectively. The UIQM is given by

$$\text{UIQM} = a \times CF + b \times CM + c \times IS \tag{18}$$

The values of weights a, b and c vary with the type of underwater images according to the application for which the underwater image is improved. For color compensation, a has more significant than b and c whereas b and c have more significant for image enhancement to improve the visibility quality. In [63] the authors consider the values of $a = 0.0282$, $b = 3.5753$ and $c = 0.2953$ and the model is significant with a P-value of 0.0339 using 30 randomly selected images for training which belong to various water conditions and depth. However, irrespective of the non-uniform values of the weights of a, b and c for both UCIQE and UIQM, we consider the values as same as used by the authors in [62] and [63].

In general, greater the values of UCIQE and UIQM correspond to an image show that the better quality of the image. A 10% increase in the value indicates that the image visual quality has increased substantially with distinguishable improvement. The estimated average values of UCIQE and UIQM for the resultant images as in Fig.6, Fig. 7,

TABLE 4. Comparison of average value of uciqe and UIQM of proposed method with existing methods.

Images	Blue		Green		Blue Green		Green Blue		Haze		Yellow	
Methods	UCIQE	UIQM	UCIQE	UIQM	UCIQE	UIQM	UCIQE	UIQM	UCIQE	UIQM	UCIQE	UIQM
TOPAL	0.5679	0.7083	0.4855	0.4132	0.5360	0.5200	0.5172	0.4970	0.5585	0.6507	0.5734	0.5606
PCDE	0.6353	**0.9548**	0.5730	0.6899	0.6121	0.7241	0.5694	0.6892	0.5691	0.7083	0.5899	0.6531
ACCE	**0.6794**	0.9369	0.6392	0.6875	0.6486	0.7492	**0.6217**	**0.7138**	0.6447	**0.8220**	0.6367	0.7185
MLLE	0.5547	0.8076	0.6017	0.7006	0.5971	0.7051	0.5599	0.6573	0.6024	0.7903	0.5982	0.6577
VCSE	0.6639	0.8739	0.6115	0.6710	0.6467	0.7400	0.5932	0.6536	0.6324	0.7877	0.6234	0.7288
TEBCF	0.6471	0.7888	0.6235	**0.7725**	0.6192	0.7008	0.6022	0.6882	0.6035	0.7627	0.6184	**0.7349**
SGUIE	0.6003	0.7563	0.5256	0.4506	0.5905	0.5884	0.5915	0.5980	0.6131	0.7437	0.6018	0.6060
Color Mixing	0.6078	0.7201	0.5903	0.5898	0.5783	0.6274	0.5452	0.5083	0.5909	0.6941	0.5939	0.5919
Proposed	0.6384	0.8515	**0.6559**	0.6652	**0.6581**	**0.7511**	0.5452	0.5083	**0.6495**	0.7476	**0.6284**	0.6113

Fig. 8, Fig. 9, Fig. 10, Fig. 11 and Fig. 12 obtained by the methods TOPAL [72], PCDE [89], ACCE [90], MLLE [66], VCSE [87], TEBCF [88], SGUIE-Net [49], Color Mixing [32] and the proposed method are given in Table 4. The best values of UCIQE and UIQM are shown in bold font. From the average values of images of each type as in Table 4, TOPAL [72] shows poor performances quantitatively whereas PCDE [89] shows better performances in terms of UIQM of 0.9548 for bluish images. Although TEBCF [88] shows poor performances qualitatively, it shows better performances quantitatively in terms of UIQM of 0.7725 and 0.7349 for greenish images and yellowish images respectively. ACCE [90] performs better in terms of UCIQE of 0.6794 and 0.6217 for bluish and greenish blue images respectively. Also, ACCE [90] performs better in terms of UIQM of 0.7138 and 0.8220 for greenish blue and haze images respectively. The proposed method outperforms well in terms of UCIQE of 0.6559, 0.6581, 0.6495 and 0.6284 for greenish, bluish green, haze and yellowish images respectively. Further, the proposed method performs well in terms of UIQM of 0.7511 for bluish green images. Hence, it is inferred that the proposed method is suitable for the enhancement of underwater images of types such as greenish, bluish, haze, yellowish and bluish green.

However, the proposed method has a limitation to solve the vision problems for the dark underwater scenes in deep sea or night time wherein artificial lighting is required to capture the images. Fig. 12 depicts the results of the proposed method for dark underwater images. The result of the proposed method for the fish image is over brightened and the red color is over compensated in case of diver image. Also, the statistical conditions for the classification of dark underwater images are not framed since all the three color channels get completely attenuated in deep sea. The light from artificial illumination is only available whereas the veiling light is not available. Hence, the proposed method needs modification for extending to dark underwater scenes. So, our future work will focus on the enhancement of the dark underwater images.

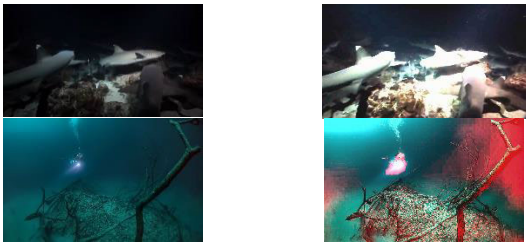

FIGURE 12. Results of the proposed method for dark underwater images.

C. ANALYSIS OF COMPUTATIONAL TIME

The computational time complexity, i.e., time taken for the enhancement of raw image having the pixel resolution of 778 × 1037 by TOPAL [72], PCDE [89], ACCE [90], MLLE [66], VCSE [87], TEBCF [88], SGUIE-Net [49], Color Mixing [32] and the proposed method are given in Table 5. The freely available non commercial trained model for SGUIE-Net [49] and TOPAL [72] are directly used for this comparative analysis. Since the trained models need graphics processor, they have been run using a separate computer configured with Intel i5 12^{th} Generation, 8GB RAM and a GPU of NVIDIA GEFORCE RTX 4GB RAM.

From TABLE 5, it is inferred that the proposed method requires less computational time to enhance the raw underwater images.

D. ABLATION STUDIES

Usually, ablation studies are conducted to analyze the contribution of a component and its importance in artificial intelligence systems. The ablation study is also conducted to investigate the importance of the proposed color correction. Fig. 13 shows the results of the proposed method with removal of one component in the overall workflow. Fig. 13(a) is the original underwater image, Fig. 13(b) is the disparity corrected image wherein the dominancy of blue color is completely removed, Fig. 13(c) is the result of Gray-World

TABLE 5. Computational time complexity for an image size of 778 × 1037 pixels.

Method	Time taken in seconds
ACCE [90]	46.45
TEBCF [88]	19.89
PCDE [89]	6.21
MMLE [66]	5.43
VCSE [87]	50.5
Color Mixing [32]	8.85
TOPAL [72]	8.11
SGUIE-Net [49]	8.9
Proposed Method	4.9

method which has red artefacts, Fig. 13(d) is the result of Gray-World with Disparity Correction which has no red artefacts, Fig. 13(e) is the result of fusion without disparity correction and has red artefacts and Fig. 13(f) is the result of fusion with disparity correction and has no red artefacts.

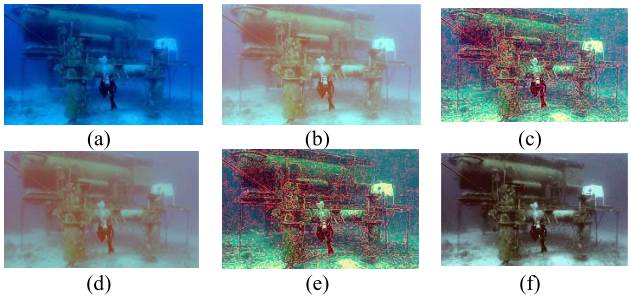

FIGURE 13. Results of ablation studies of proposed method.

From this ablation study, it is inferred that the proposed color correction reduces the red artefacts substantially when it is applied before the traditional color constancy methods.

VII. CONCLUSION

We have presented a new and simple method to enhance the degraded underwater images in this paper. The strategy uses the image statistics to estimate the rate of attenuation of light color for classification of underwater images to restore the information of degraded color channels. The experimental results shows that the quality of enhanced images obtained by the proposed method is free from yellow shades, red artefacts and block artefacts compared to the existing methods. This method does not require special hardware to enhance the images. We have depicted that the proposed approach is able to enhance all the underwater images except dark underwater images. The computational time complexity is also less compared to the state-of-the-art works. Since, the proposed method does not deal with the dark underwater images, research work will be focused on it in the future.

REFERENCES

[1] S. Ramaseshan, "*Scientific Papers of CV Raman: Volume I: Scattering of Light*. Bengaluru, Karnataka: Indian Academy of Sciences, 1988.
[2] S. Q. Duntley, "Light in the Sea," *J. Opt. Soc. Amer.*, vol. 53, pp. 214–233, Feb. 1963.
[3] F. Chilton, D. D. Jones, and W. K. Talley, "Imaging properties of light scattered by the sea," *J. Opt. Soc. Amer.*, vol. 59, no. 8, p. 891, 1969.
[4] W. H. Wells, "Loss of resolution in water as a result of multiple small-angle scattering," *J. Opt. Soc. Amer.*, vol. 59, no. 6, pp. 686–691, Jun. 1969.
[5] N. G. Jerlov, *Marine Optics* (Elsevier Oceanography Series), vol. 14, 2nd ed., Amsterdam, The Netherlands: Elsevier, 1976.
[6] H. Koschmieder, "Theorie der horizontalen sichtweite," in *Beitrage zurPhysik der Freien Atmosphare*. Leipzig, Germany: Akademische Verlagsgesellschaft Becker Erler Kom. Ges., 1924.
[7] S. Q. Duntley, A. R. Boileau, and R. W. Preisendorfer, "Image transmission by the troposphere I," *J. Opt. Soc. Amer.*, vol. 47, no. 6, p. 499, 1957.
[8] S. G. Narasimhan and S. K. Nayar, "Vision and the atmosphere," *Int. J. Comput. Vis.*, vol. 48, no. 3, pp. 233–254, 2002.
[9] R. Fattal, "Single image dehazing," *ACM Trans. Graphics (Tog)*, vol. 27, no. 3, pp. 1–9, 2008.
[10] K. He, J. Sun, and X. Tang, "Single image haze removal using dark channel prior," *IEEE Trans. Pattern Anal. Mach. Intell.*, vol. 33, no. 12, pp. 2341–2353, Dec. 2011.
[11] M. Ju, C. Ding, W. Ren, Y. Yang, D. Zhang, and Y. J. Guo, "IDE: Image dehazing and exposure using an enhanced atmospheric scattering model," *IEEE Trans. Image Process.*, vol. 30, pp. 2180–2192, 2021.
[12] C. O. Ancuti and C. Ancuti, "Single image dehazing by multi-scale fusion," *IEEE Trans. Image Process.*, vol. 22, no. 8, pp. 3271–3282, Aug. 2013.
[13] C. Li and J. Guo, "Underwater image enhancement by dehazing and color correction," *J. Electron. Imag.*, vol. 24, no. 3, Jun. 2015, Art. no. 033023.
[14] Y.-T. Peng, X. Zhao, and P. C. Cosman, "Single underwater image enhancement using depth estimation based on blurriness," in *Proc. IEEE Int. Conf. Image Process. (ICIP)*, Sep. 2015, pp. 4952–4956.
[15] C. Li, J. Quo, Y. Pang, S. Chen, and J. Wang, "Single underwater image restoration by blue-green channels dehazing and red channel correction," in *Proc. IEEE Int. Conf. Acoust., Speech Signal Process. (ICASSP)*, Mar. 2016, pp. 1731–1735.
[16] L. Chao and M. Wang, "Removal of water scattering," in *Proc. 2nd Int. Conf. Comput. Eng. Technol.*, vol. 2, Apr. 2010, pp. 35–39.
[17] N. Carlevaris-Bianco, A. Mohan, and R. M. Eustice, "Initial results in underwater single image dehazing," in *Proc. OCEANS MTS/IEEE SEATTLE*, Sep. 2010, pp. 1–8.
[18] H. Wen, Y. Tian, T. Huang, and W. Gao, "Single underwater image enhancement with a new optical model," in *Proc. IEEE Int. Symp. Circuits Syst. (ISCAS)*, May 2013, pp. 753–756.
[19] C. Qing, W. Huang, S. Zhu, and X. Xu, "Underwater image enhancement with an adaptive dehazing framework," in *Proc. IEEE Int. Conf. Digit. Signal Process. (DSP)*, Jul. 2015, pp. 338–342.
[20] Y. Ueki and M. Ikehara, "Underwater image enhancement based on the iteration of a generalization of dark channel prior," in *Proc. IEEE Vis. Commun. Image Process. (VCIP)*, Dec. 2019, pp. 1–4.
[21] A. Galdran, D. Pardo, A. Picón, and A. Alvarez-Gila, "Automatic red-channel underwater image restoration," *J. Vis. Commun. Image Represent.*, vol. 26, pp. 132–145, Jan. 2015.
[22] S. Emberton, L. Chittka, and A. Cavallaro, "Hierarchical rank-based veiling light estimation for underwater dehazing," in *Proc. Brit. Mach. Vis. Conf.*, 2015, p. 125.
[23] H.-H. Chang, "Single underwater image restoration based on adaptive transmission fusion," *IEEE Access*, vol. 8, pp. 38650–38662, 2020.
[24] B. L. McGlamery, "A computer model for underwater camera systems," *Proc. SPIE*, vol. 208, pp. 221–231, Mar. 1970.
[25] J. S. Jaffe, "Computer modeling and the design of optimal underwater imaging systems," *IEEE J. Ocean. Eng.*, vol. 15, no. 2, pp. 101–111, Apr. 1990.
[26] E. Trucco and A. T. Olmos-Antillon, "Self-tuning underwater image restoration," *IEEE J. Ocean. Eng.*, vol. 31, no. 2, pp. 511–519, Apr. 2006.
[27] P. Drews Jr., E. do Nascimento, F. Moraes, S. Botelho, and M. Campos, "Transmission estimation in underwater single images," in *Proc. IEEE Int. Conf. Comput. Vis. Workshops*, Dec. 2013, pp. 825–830.
[28] C. Ancuti, C. O. Ancuti, C. De Vleeschouwer, R. Garcia, and A. C. Bovik, "Multi-scale underwater descattering," in *Proc. 23rd Int. Conf. Pattern Recognit. (ICPR)*, Dec. 2016, pp. 4202–4207.
[29] C. O. Ancuti, C. Ancuti, C. De Vleeschouwer, and M. Sbetr, "Color channel transfer for image dehazing," *IEEE Signal Process. Lett.*, vol. 26, no. 9, pp. 1413–1417, Sep. 2019.

[30] C. O. Ancuti, C. Ancuti, C. De Vleeschouwer, L. Neumann, and R. Garcia, "Color transfer for underwater dehazing and depth estimation," in *Proc. IEEE Int. Conf. Image Process. (ICIP)*, Sep. 2017, pp. 695–699.

[31] M. Kumar and A. K. Bhandari, "Contrast enhancement using novel white balancing parameter optimization for perceptually invisible images," *IEEE Trans. Image Process.*, vol. 29, pp. 7525–7536, 2020.

[32] C. O. Ancuti, C. Ancuti, C. De Vleeschouwer, and P. Bekaert, "Color balance and fusion for underwater image enhancement," *IEEE Trans. Image Process.*, vol. 27, no. 1, pp. 379–393, Jan. 2018.

[33] C. O. Ancuti, C. Ancuti, C. De Vleeschouwer, and M. Sbert, "Color channel compensation (3C): A fundamental pre-processing step for image enhancement," *IEEE Trans. Image Process.*, vol. 29, pp. 2653–2665, 2020.

[34] Y. Tao, L. Dong, and W. Xu, "A novel two-step strategy based on white-balancing and fusion for underwater image enhancement," *IEEE Access*, vol. 8, pp. 217651–217670, 2020.

[35] E. H. Land, "The retinex theory of color vision," *Sci. Amer.*, vol. 237, no. 6, pp. 108–128, Dec. 1977.

[36] G. D. Finlayson and E. Trezzi, "Shades of gray and colour constancy," in *Proc. 12th Color Imag. Conf., Color Sci., Syst. Appl., Soc. Imag. Sci. Technol.*, 2004, pp. 37–41.

[37] M. Ebner, *Color Constancy* (Wiley-IS&T Series in Image Science and Technology). West Sussex, U.K.: Wiley, 2007.

[38] J. van de Weijer, T. Gevers, and A. Gijsenij, "Edge-based color constancy," *IEEE Trans. Image Process.*, vol. 16, no. 9, pp. 2207–2214, Sep. 2007.

[39] E. H. Land and J. J. McCann, "Lightness and retinex theory," *J. Opt. Soc. Amer.*, vol. 61, no. 1, pp. 1–11, 1971.

[40] K. Nomura, D. Sugimura, and T. Hamamoto, "Underwater image color correction using exposure-bracketing imaging," *IEEE Signal Process. Lett.*, vol. 25, no. 6, pp. 893–897, Jun. 2018.

[41] P. Liu, G. Wang, H. Qi, C. Zhang, H. Zheng, and Z. Yu, "Underwater image enhancement with a deep residual framework," *IEEE Access*, vol. 7, pp. 94614–94629, 2019.

[42] Y. Zhou, K. Yan, and X. Li, "Underwater image enhancement via physical-feedback adversarial transfer learning," *IEEE J. Ocean. Eng.*, vol. 47, no. 1, pp. 76–87, Jan. 2022.

[43] S. Wu, T. Luo, G. Jiang, M. Yu, H. Xu, Z. Zhu, and Y. Song, "A two-stage underwater enhancement network based on structure decomposition and characteristics of underwater imaging," *IEEE J. Ocean. Eng.*, vol. 46, no. 4, pp. 1213–1227, Oct. 2021.

[44] Y. Guo, H. Li, and P. Zhuang, "Underwater image enhancement using a multiscale dense generative adversarial network," *IEEE J. Ocean. Eng.*, vol. 45, no. 3, pp. 862–870, Jul. 2020.

[45] A. Dudhane, P. Hambarde, P. Patil, and S. Murala, "Deep underwater image restoration and beyond," *IEEE Signal Process. Lett.*, vol. 27, pp. 675–679, 2020.

[46] X. Xue, Z. Hao, L. Ma, Y. Wang, and R. Liu, "Joint luminance and chrominance learning for underwater image enhancement," *IEEE Signal Process. Lett.*, vol. 28, pp. 818–822, 2021.

[47] Y. Tian, Y. Xu, and J. Zhou, "Underwater image enhancement method based on feature fusion neural network," *IEEE Access*, vol. 10, pp. 107536–107548, 2022.

[48] P. Hambarde, S. Murala, and A. Dhall, "UW-GAN: Single-image depth estimation and image enhancement for underwater images," *IEEE Trans. Instrum. Meas.*, vol. 70, pp. 1–12, 2021.

[49] Q. Qi, K. Li, H. Zheng, X. Gao, G. Hou, and K. Sun, "SGUIE-net: Semantic attention guided underwater image enhancement with multi-scale perception," *IEEE Trans. Image Process.*, vol. 31, pp. 6816–6830, 2022.

[50] C. Li, C. Guo, W. Ren, R. Cong, J. Hou, S. Kwong, and D. Tao, "An underwater image enhancement benchmark dataset and beyond," *IEEE Trans. Image Process.*, vol. 29, pp. 4376–4389, 2020.

[51] R. Liu, X. Fan, M. Zhu, M. Hou, and Z. Luo, "Real-world underwater enhancement: Challenges, benchmarks, and solutions under natural light," *IEEE Trans. Circuits Syst. Video Technol.*, vol. 30, no. 12, pp. 4861–4875, Dec. 2020.

[52] D. Berman, D. Levy, S. Avidan, and T. Treibitz, "Underwater single image color restoration using haze-lines and a new quantitative dataset," *IEEE Trans. Pattern Anal. Mach. Intell.*, vol. 43, no. 8, pp. 2822–2837, Aug. 2021.

[53] E. Y. Lam, "Combining gray world and retinex theory for automatic white balance in digital photography," in *Proc. 9th Int. Symp. Consum. Electron., (ISCE)*, 2005, pp. 134–139.

[54] J. Cepeda-Negrete and R. E. Sanchez-Yanez, "Gray-world assumption on perceptual color spaces," in *Image and Video Technology* (Lecture Notes in Computer Science), vol. 8333, R. Klette, M. Rivera, and S. Satoh, Eds., Berlin, Germany: Springer, 2014.

[55] K. Iqbal, M. Odetayo, A. James, R. A. Salam, and A. Z. H. Talib, "Enhancing the low quality images using unsupervised colour correction method," in *Proc. IEEE Int. Conf. Syst., Man Cybern.*, Istanbul, Turkey, Oct. 2010, pp. 1703–1709.

[56] C. G. L. Rafael and R. E. Woods, *Digital Image Processing*, 4th ed., London, U.K.: Pearson, 2018.

[57] S. M. Pizer, R. E. Johnston, J. P. Ericksen, B. C. Yankaskas, and K. E. Müller, "Contrast-limited adaptive histogram equalization: Speed and effectiveness," in *Proc. 1st Conf. Vis. Biomed. Comput.*, 1990, p. 2.

[58] S.-C. Pei and C.-Y. Chen, "Underwater images enhancement by revised underwater images formation model," *IEEE Access*, vol. 10, pp. 108817–108831, 2022.

[59] S. Jin, P. Qu, Y. Zheng, W. Zhao, and W. Zhang, "Color correction and local contrast enhancement for underwater image enhancement," *IEEE Access*, vol. 10, pp. 119193–119205, 2022.

[60] C.-Y. Li, J.-C. Guo, R.-M. Cong, Y.-W. Pang, and B. Wang, "Underwater image enhancement by dehazing with minimum information loss and histogram distribution prior," *IEEE Trans. Image Process.*, vol. 25, no. 12, pp. 5664–5677, Dec. 2016.

[61] C. Li, S. Anwar, and F. Porikli, "Underwater scene prior inspired deep underwater image and video enhancement," *Pattern Recognit.*, vol. 98, Feb. 2020, Art. no. 107038.

[62] M. Yang and A. Sowmya, "An underwater color image quality evaluation metric," *IEEE Trans. Image Process.*, vol. 24, no. 12, pp. 6062–6071, Dec. 2015.

[63] K. Panetta, C. Gao, and S. Agaian, "Human-visual-system-inspired underwater image quality measures," *IEEE J. Ocean. Eng.*, vol. 41, no. 3, pp. 541–551, Jul. 2016.

[64] K. Simonyan and A. Zisserman, "Very deep convolutional networks for large-scale image recognition," 2014, *arXiv:1409.1556*.

[65] W. Zhang, Y. Wang, and C. Li, "Underwater image enhancement by attenuated color channel correction and detail preserved contrast enhancement," *IEEE J. Ocean. Eng.*, vol. 47, no. 3, pp. 718–735, Jul. 2022.

[66] W. Zhang, P. Zhuang, H.-H. Sun, G. Li, S. Kwong, and C. Li, "Underwater image enhancement via minimal color loss and locally adaptive contrast enhancement," *IEEE Trans. Image Process.*, vol. 31, pp. 3997–4010, 2022.

[67] W. Song, Y. Wang, D. Huang, A. Liotta, and C. Perra, "Enhancement of underwater images with statistical model of background light and optimization of transmission map," *IEEE Trans. Broadcast.*, vol. 66, no. 1, pp. 153–169, Mar. 2020.

[68] R. Cong, W. Yang, W. Zhang, C. Li, C.-L. Guo, Q. Huang, and S. Kwong, "PUGAN: Physical model-guided underwater image enhancement using GAN with dual-discriminators," *IEEE Trans. Image Process.*, vol. 32, pp. 4472–4485, 2023.

[69] N. Wang, T. Chen, X. Kong, Y. Chen, R. Wang, Y. Gong, and S. Song, "Underwater attentional generative adversarial networks for image enhancement," *IEEE Trans. Hum.-Mach. Syst.*, vol. 53, no. 3, pp. 490–500, Jun. 2023.

[70] K. Panetta, K. M. S. Kamath, S. P. Rao, and S. S. Agaian, "Deep perceptual image enhancement network for exposure restoration," *IEEE Trans. Cybern.*, vol. 53, no. 7, pp. 4718–4731, Jul. 2023.

[71] S. Yan, X. Chen, Z. Wu, M. Tan, and J. Yu, "HybrUR: A hybrid physical-neural solution for unsupervised underwater image restoration," *IEEE Trans. Image Process.*, vol. 32, pp. 5004–5016, 2023.

[72] Z. Jiang, Z. Li, S. Yang, X. Fan, and R. Liu, "Target oriented perceptual adversarial fusion network for underwater image enhancement," *IEEE Trans. Circuits Syst. Video Technol.*, vol. 32, no. 10, pp. 6584–6598, Oct. 2022.

[73] K. Li, L. Wu, Q. Qi, W. Liu, X. Gao, L. Zhou, and D. Song, "Beyond single reference for training: Underwater image enhancement via comparative learning," *IEEE Trans. Circuits Syst. Video Technol.*, vol. 33, no. 6, pp. 2561–2576, Jun. 2023.

[74] M. Li, K. Wang, L. Shen, Y. Lin, Z. Wang, and Q. Zhao, "UIALN: Enhancement for underwater image with artificial light," *IEEE Trans. Circuits Syst. Video Technol.*, vol. 33, no. 8, pp. 3622–3637, Aug. 2023.

[75] J. Tian, X. Guo, W. Liu, D. Tao, and B. Liu, "Deformable convolutional network constrained by contrastive learning for underwater image enhancement," *IEEE Geosci. Remote Sens. Lett.*, vol. 20, pp. 1–5, 2023.
[76] N. Qiao, L. Dong, and C. Sun, "Adaptive deep learning network with multi-scale and multi-dimensional features for underwater image enhancement," *IEEE Trans. Broadcast.*, vol. 69, no. 2, pp. 482–494, Jun. 2023.
[77] J. Hao, H. Yang, X. Hou, and Y. Zhang, "Two-stage underwater image restoration algorithm based on physical model and causal intervention," *IEEE Signal Process. Lett.*, vol. 30, pp. 120–124, 2023.
[78] H. Yan, Z. Zhang, J. Xu, T. Wang, P. An, A. Wang, and Y. Duan, "UW-CycleGAN: Model-driven CycleGAN for underwater image restoration," *IEEE Trans. Geosci. Remote Sens.*, vol. 61, 2023, Art. no. 4207517.
[79] L. Peng, C. Zhu, and L. Bian, "U-shape transformer for underwater image enhancement," *IEEE Trans. Image Process.*, vol. 32, pp. 3066–3079, 2023.
[80] X. Liu, S. Lin, K. Chi, Z. Tao, and Y. Zhao, "Boths: Super lightweight network-enabled underwater image enhancement," *IEEE Geosci. Remote Sens. Lett.*, vol. 20, pp. 1–5, 2023.
[81] J. Zhou, L. Pang, D. Zhang, and W. Zhang, "Underwater image enhancement method via multi-interval subhistogram perspective equalization," *IEEE J. Ocean. Eng.*, vol. 48, no. 2, pp. 474–488, Apr. 2023.
[82] Y. Zhong, J. Wang, and Q. Lu, "SCAUIE-net: Underwater image enhancement method based on spatial and channel attention," *IEEE Access*, vol. 11, pp. 72172–72185, 2023.
[83] G. Han, M. Wang, H. Zhu, and C. Lin, "UIEGAN: Adversarial learning-based photorealistic image enhancement for intelligent underwater environment perception," *IEEE Trans. Geosci. Remote Sens.*, vol. 61, 2023, Art. no. 5611514.
[84] N. Qiao, J. Sun, Q. Ge, and C. Sun, "UIE-FSMC: Underwater image enhancement based on few-shot learning and multi-color space," *IEEE Trans. Circuits Syst. Video Technol.*, vol. 33, no. 10, pp. 5391–5405, Oct. 2023.
[85] R. Chen, Z. Cai, and J. Yuan, "UIESC: An underwater image enhancement framework via self-attention and contrastive learning," *IEEE Trans. Ind. Informat.*, vol. 19, no. 12, pp. 11701–11711, Dec. 2023.
[86] Q. Chen, Z. Zhang, and G. Li, "Underwater image enhancement based on color balance and multi-scale fusion," *IEEE Photon. J.*, vol. 14, no. 6, pp. 1–10, Dec. 2022.
[87] X. Li, G. Hou, L. Tan, and W. Liu, "A hybrid framework for underwater image enhancement," *IEEE Access*, vol. 8, pp. 197448–197462, 2020.
[88] J. Yuan, Z. Cai, and W. Cao, "TEBCF: Real-world underwater image texture enhancement model based on blurriness and color fusion," *IEEE Trans. Geosci. Remote Sens.*, vol. 60, 2022, Art. no. 4204315.
[89] W. Zhang, S. Jin, P. Zhuang, Z. Liang, and C. Li, "Underwater image enhancement via piecewise color correction and dual prior optimized contrast enhancement," *IEEE Signal Process. Lett.*, vol. 30, pp. 229–233, 2023.
[90] X. Li, G. Hou, K. Li, and Z. Pan, "Enhancing underwater image via adaptive color and contrast enhancement, and denoising," *Eng. Appl. Artif. Intell.*, vol. 111, May 2022, Art. no. 104759.
[91] M. Kanagavel and V. Thanikaiselvan, "Adjustment of pixel intensity for removal of color casts in underwater images," *IEEE Access*, vol. 12, pp. 32266–32277, 2024.
[92] W. Wang, D. Yan, X. Wu, W. He, Z. Chen, X. Yuan, and L. Li, "Low-light image enhancement based on virtual exposure," *Signal Process., Image Commun.*, vol. 118, Oct. 2023, Art. no. 117016.

M. KANAGAVEL was born in Virudhunagar, Tamil Nadu, India, in 1990. He received the Bachelor of Engineering degree in electronics and communication engineering and the Master of Engineering degree in communication systems from Anna University, Chennai, Tamil Nadu. He is currently pursuing the Doctor of Philosophy degree in electronics and communication engineering with Vellore Institute of Technology, Vellore, India. His research interests include image processing for the enhancement of underwater images, low light illuminated images, and hazy images.

V. THANIKAISELVAN (Member, IEEE) received the B.E. degree in electronics and communication engineering form Bharathidasan University, Trichy, in 2002, the M.Tech. degree in advanced communication systems from SASTRA University, Thanjavur, in 2006, and the Ph.D. degree in the field of image steganography for information security form Vellore Institute of Technology (VIT), Vellore, Tamil Nadu, India, in 2014. He is currently working as a Professor with the Department of Communication Engineering under the School of Electronics Engineering, VIT. So far, he has published more than 100 research articles in peer reviewed Scopus indexed journals and conference papers. He has produced seven Ph.D. candidates. Currently he is guiding four Ph.D. candidates in the areas of Information Security and Digital Image Processing. He is an active IEEE member and reviewer for Elsevier, Wiley, and springer journal.